Abstract

Ensuring the full connection between steel sheet and concrete after applying a load to composite slabs is still nowadays something difficult to achieve. The aim of the current project is to reveal the experimental results of a new bonding system, under patent [19] by the Universitat Politècnica de Catalunya (UPC) which its function is to resist the shearing forces and separating forces generated between both materials when the composite steel-concrete element is loaded ensuring the commented full connection between materials and working as a composite cross section.

The new method has been validated with amount of tests which results have been compared with different commercial carbon steel sheeting slabs and ferritic stainless steel sheeting slabs, all of them with traditional embossment as a connection system. These tests have been carried out in “Laboratori d’estructures i resistència de materials” (LERMA)[2][3]. The comparison between composite slabs using traditional embossments and those which use new connection system is extremely deep. The ultimate state values of new composite slabs were reached with inexistent slippage, so the ultimate bending moment resistance is higher on new composite slabs.

Moreover, theoretical predicted calculations, always by the Eurocode4[4]directions, have been done trying to predict the ultimate state service for each studied composite slab. Then it has been compared such predicted results with the experimental testing.
Comparison of experimental and analytical results of the load-carrying capacity of composite slabs revealed that agreements between these values are sufficiently good.

Index

1. Glossary

Nomenclature

A_p : *Nominal sheet area*

A_{pe} *: Effective area of the sheet in tension*

A_s *: Effective area of passive reinforcement tensioned*

b : Width of the resistant section

b_0 *: Average width of the nerves*

b_c *: Average width of concrete compressed zone*

d : Distance between the upper edges of the concrete to the underside of the nerve sheet.

d_p *: Distance from the top edge of the slab to the centroid of the effective area of the steel*

d_s *: Height of center of gravity of reinforcement compared to the base plate*

E: Young modulus

e : Distance from the centroid of the effective area of the sheet to the bottom edge

e_p *: Distance from the plastic neutral axis of the effective area of the sheet to the bottom edge*

NPF : Neutral plastic fiber

f_{ck} *: Nominal strength of concrete*

f_{ct} *: Cylinder compressive strength of concrete*

f_{yu} *: Maximum yield stress of steel*

f_{yp} *: Nominal yield characteristic of steel*

f_{ys} *: Yield strength of tensioned reinforcement*

h_c *: Height of concrete slab*

k : Coefficient k of the m-k method

L : Length of the slab

l_{bc} : Length of the concrete support

l_{bs} : Length of the steel support

L_s : Length into shear span

m: Coefficient m of the m-k method

$M_{pl\,Rd}$: Last plastic torque

M_{ed} : Calculated maximum torque

M_{pa} : Calculated plastic torque resistance

M_{pr} : Reduced plastic torque of the steel

M_{Rd} *:* Design resistance Torque

N_{cf} : Concrete compression resultant

N_c: Concrete compression

N_p : Sheet tension resultant

N_s : Resulting from tension in passive reinforcement

s : Width of the pattern sheet

t : Steel sheeting width

T_c: Stiffness multiplier for cracked tensile condition

$V_{L,Rd}$, : Last shear resistance

V_t : Maximum shear strength on the PSC method

x_{pl} : Depth of the plastic neutral axis

z : Resulting mechanical arm between concrete and steel

Greek symbols

γ_{ac} : Safety factor for Steel

γ_c: Partial safety factor of concrete

γ_s : Partial safety coefficient for the ultimate limit state

η: Partial connection factor of the slab

μ : Friction coefficient

v: Poison's coefficient

τ_{Rk} : Characteristic longitudinal shear resistance

τ_u : Longitudinal shear resistance

τ_m : Average resistance to longitudinal shear

2. Preface

2.1. Origins

Composite slabs consisting of profiled steel sheeting, reinforcement and concrete, are widely used in the building industry in the last decades due to composite slabs systems provide permanent and integral reinforcement, which eliminates the need for placing and stripping of plywood and timber formwork which reduces the construction time and dead-load, both of the main interests in high rise steel frame building.
Composite slabs have been also introduced recently to consider the increase in strength that can be achieved if the profiled steel sheeting is taken into account in strength calculations and it has meant a development against reinforced concrete framed constructions.
The application of the combination of profiled steel sheeting to existent concrete slabs was first developed in America in the early 1950s. Following its introduction into the United Kingdom in the 1970s was become one of the most common forms of floor system for steel framed buildings. In Australia, in the early 1990's much research was carried out using the same construction technique in beams also.

From most of tests and old studies, it is known that the load carrying capacity of composite slabs is normally dictated by the shear bond, between the steel sheeting and the concrete, rather than yielding from the decking. This shear bond generally breaks down when there is one relative displacement between the steel sheeting and the concrete, called slip, which use to be occurred at the ends of the span.

So the need of avoiding the slippage of the concrete through the steel deck is the most important goal when it is studied and formed the composite slabs floors.

2.2. Motivation

The researching in this project is motivated due to the interests of the author in the construction field due to an internship carried out in Germany where a big mall structure was built, accompanied by a motivation created by the professor Miquel Ferrer, who has been studying the composite slabs behaviour for the last decade.

Moreover, the combination between the introduction into the structures field by the author and a new method to connect the components in still not studied slabs, which can be a revolution in this field, are two additional motivations in order to research in this project.

3. Introduction

3.1. The aim of the project

The aim of this research is to reveal the experimental results of a new bonding system, under patent by the Universitat Politècnica de Catalunya (UPC)[2], ensuring the full connection between steel sheet and concrete, and are compared with the behavior of composite slabs with traditional embossments created by different types of steel sheets.[3]

Another objective of the research tries to isolate the different components of the connection in order to establish the importance of each one, studying tests that were already performed in other projects, and tested during the experimental program part of this project. These long span systems require investigation of new deck profiles that can be used to provide an adequate interaction with the concrete slab.

Deflection and ultimate state service calculations of the composite slabs with the new connection have been carried out and compared with the experimental case. These calculations have been easily described due to the perfect composite action on the cross-section of the new composite slabs.

3.2. The scope of the project

The scope of the project tends to compile, analyze and deal with the database of the bending tests of two different commercial steel sheeting profil·les (ferritic stainless steel sheeting and galvanized steel sheeting) with different connection systems to the concrete, tested at “Laboratori d´estructures I Resistencia de materials” (LERMA) in the UPC, including in two of them the new patent connection system.

Additionally, It has been also described all materials used on tests, including their properties. Following the procedure described in Eurocode 4 theoretical formulations for its calculation and verification has been also carried out in order to evaluate the ultimate limit state on slabs with the new connection system. The project also reveals the description of test set-up and the testing procedure on the mentioned composite slabs. The purpose of the project is not modelling with the help of Finite Elements, neither are calculations or design of traditional embossed composite slabs.

4. Main features of composite slabs

Composite slabs are structural bidimensional elements which are commonly submitted to bending stresses. It consists of cold formed steel sheeting, usually between 0.75 and 1.3 mm thick, cast concrete, and it might include steel reinforcement situated between top and bottom of the thickness.

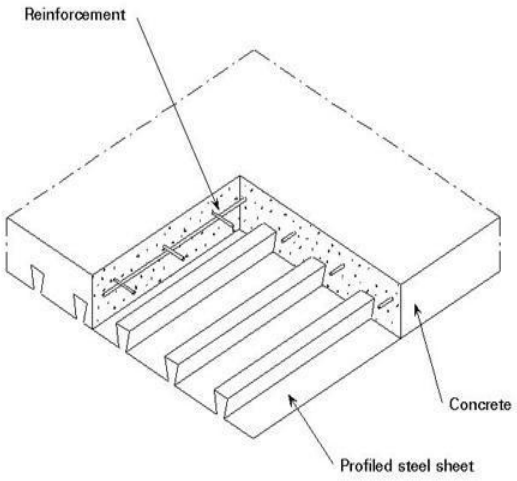

Figure1 Composite slab materials[1]

Improvement in efficiency of composite floor systems can be obtained directly by optimization of materials before mentioned, which includes the possibility of developing longer span composite slab systems. Characteristics of the three main elements composed in the composite slabs are described in the following sections.

4.1. Comparison with the conventional reinforced concrete slabs

Composite slab system have some advantages against the conventional reinforced concrete slabs.

Firstly, composite slabs provide horizontal stiffness over the structure, acting as a diaphragm side and helping the transmission of such loads, eliminating thus the riostes need to use in

the construction phase.

Secondly, it acts as an astensile reinforcement. This eliminates or significantly reduces the need for tensile reinforcement. The other form of reinforcement required is the wire mesh which is used to control temperature and shrinkage. In addition, the shape of steel deck leads to a reduced amount of concrete, as a result of a lighter structure with reduced column sizes and smaller and simpler foundation loads. This contributes to a reduction in material costs and an increase in construction speed and a shorter project duration, which leads to reduced costs in terms of construction management services.

Finally it also permits avoiding the need of use shoring systems during the construction stage, facilitating movement between plants and offering open plan spaces as well as the steel sheeting also works as a steady platform in construction progress and it is used as a formwork while concrete is pouring. The use of steel also facilities an earlier start to the operations of the building, therefore requiring shorter periods for the recovery of construction costs. The fact that steel quality is not compromised by bad weather conditions allows for a faster erection process, reducing any potential delays and associated costs during construction.

Despite the fact that there are amount of advantages, forged steel frames collaborates also have a disadvantage: its fire behaviour is worse than conventional reinforced concrete floors fire behaviour. The reason for this is the decreasing in resistance to traction of steel when it is exposed to fire, and due to concrete is not a material capable to support it, there is a rapid collapse between the composite slab materials.

4.2. Steel sheeting

The main structural function of the steel decking is to act compositely with the concrete to support the loads on the floor.

The effect of cold-rolling on the material properties of the sheeting must also be taken into account in the folds of the sheeting. As main effects of the folds over the material are considered increasing yield and ultimate strengths, loss of yielding plateau, and decrease in ductility.

These effects depend commonly on the magnitude of the plastic strains caused by the

forming process composite action which is obtained by shear bond, mechanical interlock and friction between the concrete and the decking. In order to achieve this interaction are used to roll embossments over the steel sheet and amount of re-entrant parts in the deck profile, which prevent the separation between the steel sheet and concrete, similar to the deformations formed in rebar used in a traditional reinforced concrete slab.

4.2.1. Profiled steel sheeting

There are two generic types of shallow steel decking: re-entrant (dovetail) profiles and open ribbed profiles.

Dovetailed profiles are used due to the shrinkage effect where a friction interlock is created, this fact creates a tightly embracement between the concrete and the plate.

However, this configuration with all reentrants shape over the sheet, make increase the steel material, and it makes as a direct consequence, decking more expensive. Even if the steel sheeting is open ribbed or closed, it usually has embossments or indentations to improve its resistance to longitudinal shear tensions in concrete-steel interface and enhance the joint behavior.

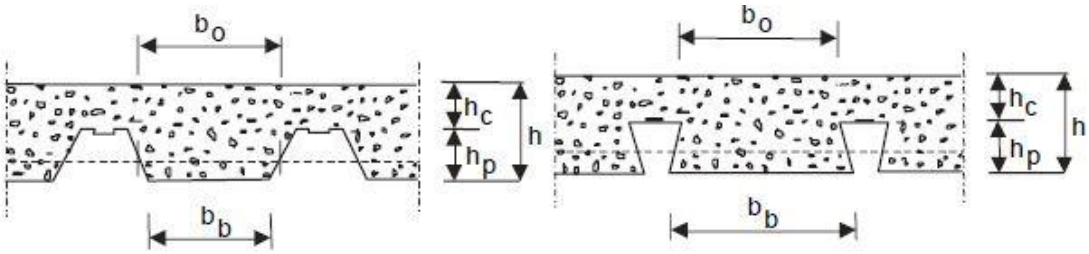

Figure 2 Open ribbed profile (left) and dove tail profile (right) [1]

4.2.2. Characteristics of the deck

This material is available with yield strengths (f_{yp}) ranging from 235 N/mm^2 to at least 400 N/mm^2, and profiles with depths ranging from 45mm to over 200 mm. Net width of the deck (b) between 700 mm and 900 mm and with a wide range of shapes.

The total specimens which permit achieving composite action with concrete are carried out with a steel sheet between 0.75 to 1.5 mm thickness (t) and a distance between ribs d_n of 150 to 300 mm.

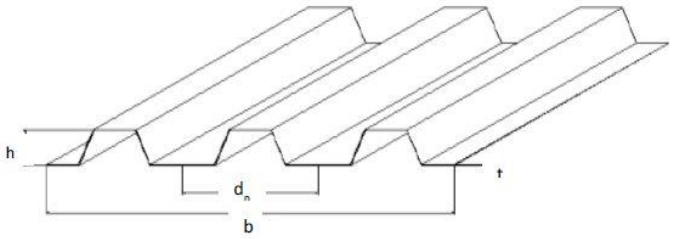

Figure 3 Common parameters of steel sheeting

4.2.3. Makeup of the steel sheeting

Most common steel decking are made by galvanized method which consists on applying a zinc coating to profile deck. Normally is enough with a total covering of 275 g/m² and 0.02mm extra thickness for each part. The steel sheeting is cold-formed from a carbon steel coil which profile is progressively formed due to the action of some rollers.

Figure 4 Steel sheeting conformation.[7]

4.3. Concrete

Concrete is a mixture of cement paste and aggregate, each of which has an essentially linear and brittle stress-strain relationship in compression. Brittle materials tend to develop tensile fractures perpendicular to the direction of the largest tensile strain.

Thus when concrete is subjected to uniaxial compressive loading, cracks tend to develop parallel to the maximum compressive stress.

Two different types of concrete are used in composite slab, normal weight concrete and lightweight concrete, but in the Eurocodes these are now referred to as normal concrete and lightweight aggregate concrete respectively. Normal concrete is made by dense aggregates from natural sources. Lightweight aggregate concrete contains artificially aggregates such as

expanded pulverised fuel ash pellets.

Eurocode 4[4] accepts only concrete qualities above C20/C25 for normal and between LC20/22 and LC60/66 for lightweight concrete.

Concrete used for the specimens is of normal weight, where the characteristic compressive strengths at 28 days is 26,86 N/mm2. Concrete's degree affects the stiffness of the composed section and the shear tensions on the connectors.

			C20/25	C25/30	C30/37	C35/45	C40/50	C45/55	C50/60
f_{ck}	12	16	20	25	30	35	40	45	50
f_{ctm}	1,6	1,9	2,2	2,6	2,9	3,2	3,5	3,8	4,1
$f_{ctk\ 0,05}$	1,1	1,3	1,5	1,8	2,0	2,2	2,5	2,7	2,9
$f_{ctk\ 0,95}$	2,0	2,5	2,9	3,3	3,8	4,2	4,6	4,9	5,3

Table 1 Normal concrete values from compressive and tensile strengths resistance .

Table 2 represents the nominal values from secant modulus of elasticity of concrete :

Classe Formigó (o f_{ck})	(12)	(16)	C20/25	C25/30	C30/37	C35/45	C40/50	C45/55	C50/60
E_{cm}	26	27,5	29	30,5	32	33,5	35	36	37

Table 2 Secant modulus of elasticity of concrete.

4.4. Reinforcement

The bar reinforcement in composite slabs usually takes the form of a relatively light welded fabric, commonly supplemented by some bar reinforcement. The fabric reinforcement is required to perform a number of functions:

- Provide bending resistance at the supports of the slab in the fire condition (this reinforcement is usually ignored under 'normal' load conditions).
- Reduce and control cracking at the supports, which occurs because of flexural tension and differential shrinkage effects.
- Distribute the effects of localised point loads and line loads.
- Strengthen the edges of openings.

5. Behavior characteristics

5.1. Behavior based on materials interaction

In order to create an efficient composite slab, as a mix structural element, is essential to know and understand how it behaves after external loads which it has to support. The behavior of composite slabs in front of tangential stresses depends on the capacity of materials to transmit gradient efforts. This is known as degree of interaction

The interaction between these materials could be described as total, partial, or inexistent depending on the relative movement of concrete through the steel sheeting and the shear bond that appears between their contact surfaces.

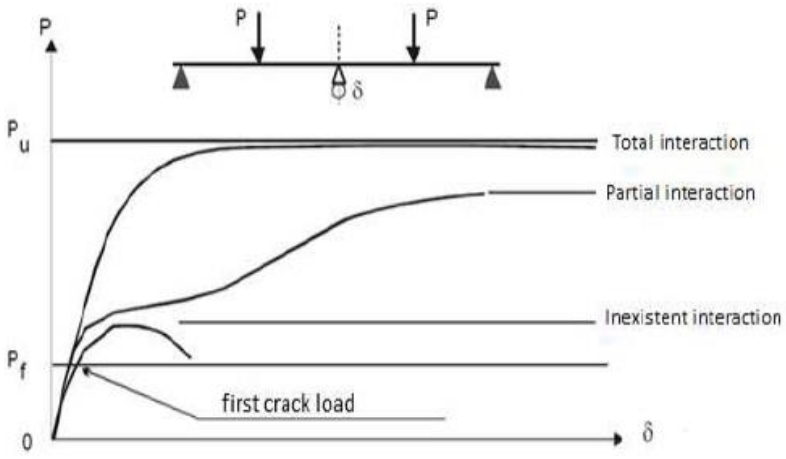

Figure 5 Steel-concrete interaction [8]

5.1.1. Total interaction

Total interaction appears when the contact between the different surfaces is perfect and continuous through all over surfaces on the span. There is no slippage or relative movement between the two materials and it can be accepted as valid the hypothesis of longitudinal continuity deformation between materials. It is also assumed the linear law deformation and all structural and all structural elements work together as a single element.

In this case bending will produce the failure due to the exhaustion of the steel sheeting.

A possible working situation in total connection where the concrete is fissured and steel works in elastic range, it is shown in figure

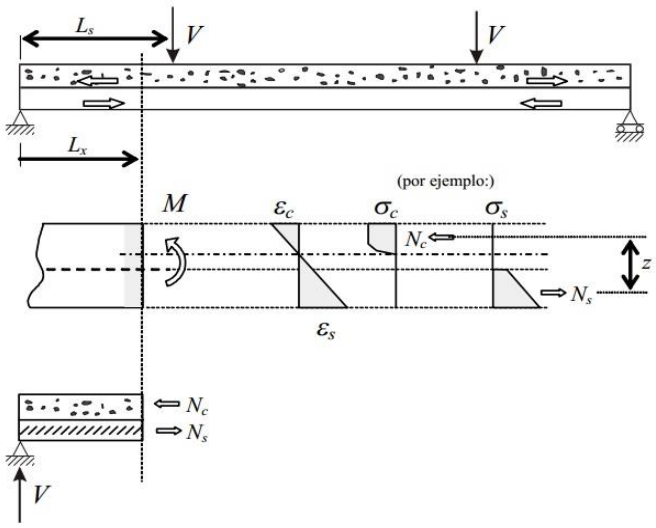

Figure 6 Total connection diagram[8].

The average force for embossment patron in the distance L_s is :

$$F_{emb} = \frac{N_c}{number\ of\ embossments} = \frac{V L_s/_z}{L_s/_z} = V\frac{s}{z} \qquad \text{(Eq. 5.1)}$$

Where, s is the distance between embossments patron

z is the lever arm of longitudinal resultants

5.1.2. Partial interaction

Partial interaction between steel and concrete is produced when there is a limited slippage between materials. Deflection is not the same for both materials and there is a longitudinal shear transmission between their contact surfaces, affecting its resistant capacity. Moreover, in the absence of continuity of deformation between the elements, the respective neutral axis do not coincide. This failure is usually produced as a consequence of longitudinal shear and the ultimate load is lesser than the total interaction one. Bankruptcy can be ductile or brittle.

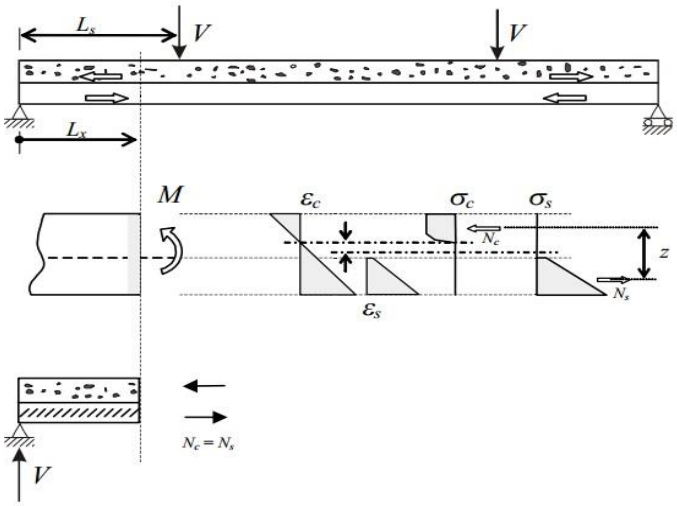

Figure 7 Partial connection diagram[8].

5.1.3. Inexistence interaction

When there is inexistence interaction between materials, there is a free slippage without limitations and there is no transmission of stresses. It could be considered inexistent composite behavior as a sum of independent parallel structural elements, therefore ultimate load is fewer than in the other cases. Obviously, in this case, the contribution of the steel sheet has a negligible effect on the composite flexure, acting only as formwork.

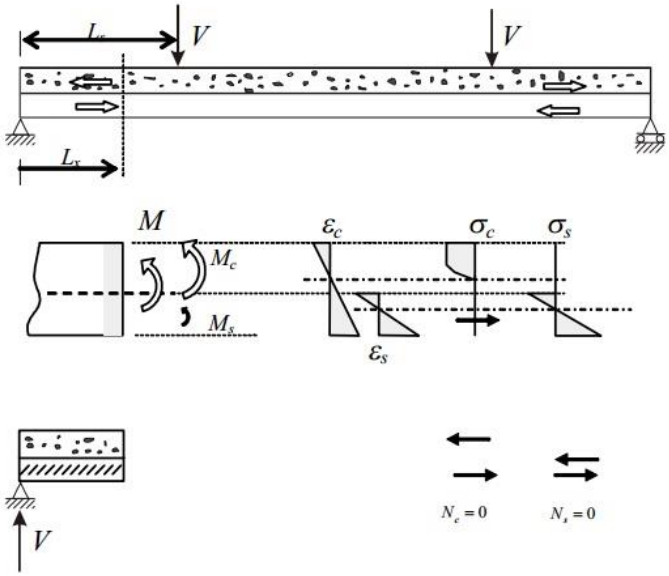

Figure 8 Inexistent connection diagram[8].

5.2. Connection mechanisms

In response to the need of avoiding the slippage of the concrete through the steel deck which is the most important goal, there are three types of shear connection between the profiled steel sheet and a concrete slab.

The first type of shear connection is known as 'frictional' interlock, which it is proved that when the load is bending the slab, slippage occurs frequently.

The second type of shear connection is 'end anchorage'. This can be provide where the end of a sheet rests on a steel beam, by means of shot-fired pins, or by welding studs through the sheeting to the steel flange.

Finally the third type, which is the most common used, is the mechanical interlock, which is entrusted to a repeating pattern of embossments all along the ribs of the sheet. Its function is the same as corrugations on reinforcing bars for concrete. The effectiveness of these embossments depends entirely on their depth which must be accurately controlled manufacture.

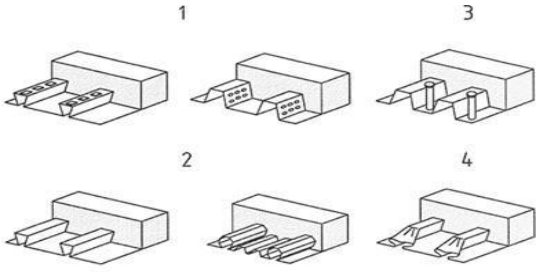

Key
1 mechanical interlock
2 frictional interlock
3 end anchorage by through-deck welded studs
4 end anchorage by deformation of the ribs

Figure 9 Types of mechanical interlock[1].

5.2.1. Embossments problem

The traditional embossments wedge effect transforms the longitudinal slip into forces on steel sheet that mainly causes the transversal bending of steel sheet , presenting a much lower stiffness, and posterior vertical separation of both elements when slip is high enough to release them , and the consequently load drop .

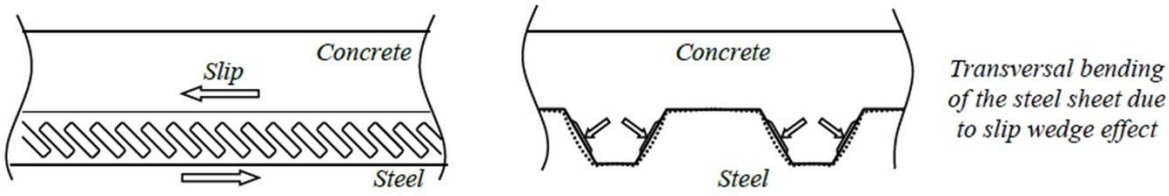

Figure 10 Transversal bending[10]

A possible equilibrate state is shown in figure 11. The ends of the embossments, position 1, are the main contributors to the resistance to slippage between materials. Forces produced by the presence of embossments which act as physical obstacles over the concrete, can be splitted into two components. The first component is the longitudinal direction and the second component, which is assumed to act perpendicular to the web.

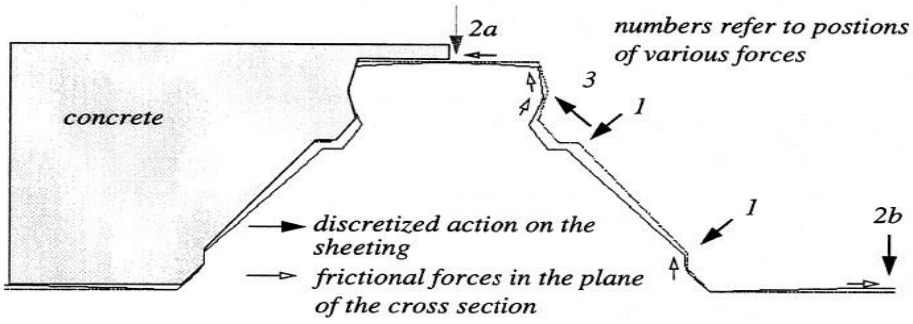

Figure 11 Possible equilibrate state[18]

Compressive vertical forces arise at the contacts between the concrete and the flanges which tend to lift the concrete from the sheeting.

The position of the vertical forces on the concrete, position 2a and position 2b, depends on the sheeting profile, and on the direction and distribution of actions on the web.

The force at position 3 additionally to the frictional forces increase due to the slip between concrete and sheeting. The force at position 3 can be named as splitting force because its tendency is making split the concrete. Depth, position on the sheet and volume from embossments are dependent characteristics from these splitting forces. This splitting force can be so high that it might cause splitting concrete which originates a peak of the reentrant portion.

5.2.2. The new UPC connection system

The new connection system, under patent by UPC, achieves the full connection of the steel sheet to concrete surface by a series of many small crown-shaped breakages generated in the steel sheet by a mechanism illustrated in next figure. These breakages are oriented towards the side of the sheet which will be contacting the concrete, these small breakages have the function to transfer shear forces between both materials once they are inserted into the concrete when it is poured.

Figure 12 Square punch[2].

Figure 13 Punch mechanism[2].

Another interesting point of this new connection system is the small size and the number of the crowns, distributed uniformly over the sheet, which makes that the shear forces are not totally concentrated in specific points; such like the only-friction or the rusted-surface mechanisms. Both local breakage of the concrete and excessive deformation of the projections themselves is thus prevented.

On the other hand, its effectiveness also resides in the complete and through punching, when the breakage is as open as possible traverse the steel sheet completely. Thus, such a breakage does not lead to the detachment of both materials since there is no wedge effect between them, unlike embossments do.

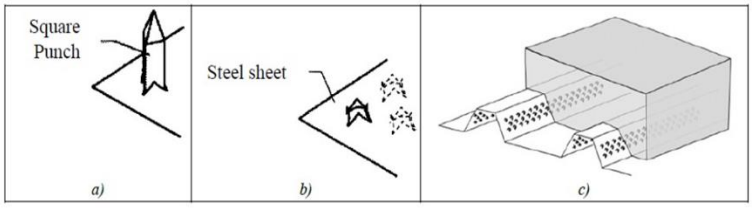

Figure 14 Method summarized[2]

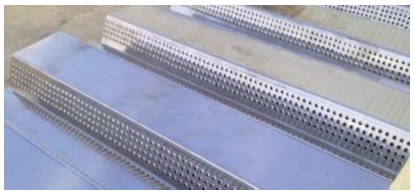

Figure 15 Resulting breakage.

5.3. Failure mechanisms

The shear bond characteristic depends on many factors such as the height or shape.

It could be described the main failures in the design of composite floors in Eurocode 4, which is based on experimental results obtained for simply supported composite slabs loaded with two line loads, as follows:

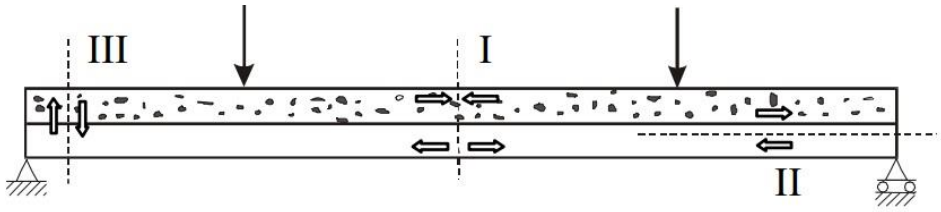

Figure 16 Main failures position[1].

The flexural failure occurs when complete interaction at the interface between concrete and steel is achieved, and where the strength and ductility of the mechanical interlocking do not limit the flexural capacity. This type of failure usually occurs in long thin slabs. The reason why it occurs is the application of an excessive torque ($M_{pl,Rd}$) which it is higher than the resistance of the slab.

When the failure mode is due to longitudinal shear; the ultimate load resistance is reached at the steel interface. This happens in section II along the shear span L_S, where apart from horizontal shear forces, bending action can also create vertical separation between the steel and the concrete. Therefore, the profiled sheeting must resist vertical separation as well as transfer horizontal shear forces between the steel-concrete interfaces.

Failure III is an unusual mechanism of failure, and has a type of brittle rupture with small deformations and cracks appearing at 45 ° in the middle plane of the slab.

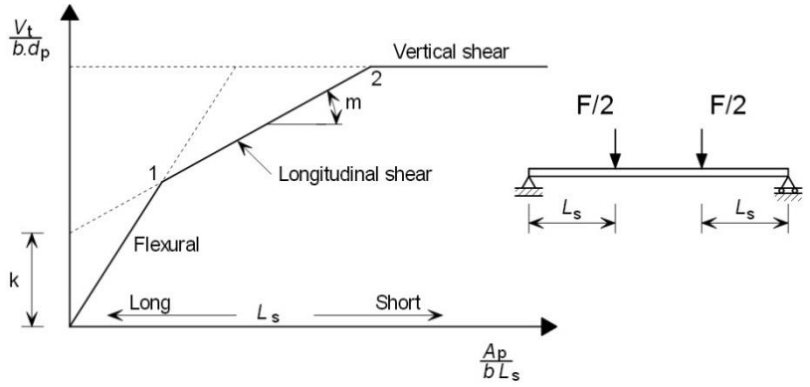

Figure 17 Modes of Failure of Composite slabs depending on length[1]

5.4. Resistance of composite slabs to different failure modes

5.4.1. Verification of the sagging bending resistance

In previous section have been explained different possible types failures when the slab is loaded, as a failure mode owing to sagging bending resistance it has been studied the type failure I. That failure mode is reached whether the steel sheeting yields in tension or if concrete reaches to its compression resistance.

One of the assumptions of this failure mode is to ensure the complete interaction at the interface between concrete and steel, therefore this is going to be the case of study related to composite slabs with the new connection system.

As a design strength ultimate limit state is considered:

Profiled steel $f_{yp,d} = \frac{f_{yp}}{\gamma_M}$

Concrete $0.85 f_{cd} = 0.85 \frac{f_{ck}}{\gamma_C}$

Reinforced steel $f_{sd} = \frac{f_{sk}}{\gamma_s}$

Additionally, when tension reinforcement or anti-cracking reinforcement is added into the depth of the concrete slab, this reinforcement is generally neglected when it is evaluating resistance to sagging bending.

There are two different ways to calculate the ultimate limit state when this failure occurs in the slab. One of them is the most common case where the neutral axis for bending lies in the concrete, and the other case, which usually happens when the sheeting is unusually deep, the neutral axis is situated in the steel sheeting.

With the aim to know in which situation is situated, firstly it is compared the resulting compression force in the concrete N_{cf} with the tension force Np in the steel sheeting, and when N_{cf} value is higher than Np then the neutral axis is above the sheeting. Otherwise the neutral axis is situated in the steel sheeting web.

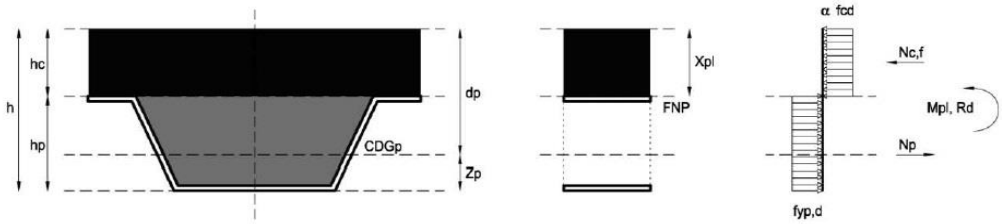

Figure 18 Neutral axis situated in hp high[14]

$$N_{cf} = \alpha f_{cd} b h_c \qquad \text{(Eq. 5.2)[4]}$$

$$N_p = A_{pe} f_{yb} \qquad \text{(Eq. 5.3)[4]}$$

If $N_{cf} > N_p$ Neutral axis above the sheeting

If $N_{cf} < N_p$ Neutral axis in the sheeting

Neutral axis above the sheeting

The stress distribution for sagging bending is shown in Figure 18. There must be full shear connection, so the resulting tension force N_p in the steel sheeting, which is calculated with the characteristics of the effective steel section A_{pe}, is equal to the resulting compression force in the concrete N_{cf} corresponding to the force acting on the width b of the slab, and the distance x_{pl}. Moreover, as it is shown in the distribution of the figure, the tension resistance of the concrete is taken as a 0.

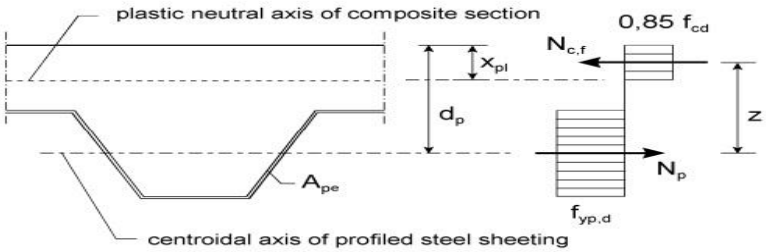

Figure 19 Stress distribution for sagging bending neutral axis above the steel sheet [14]

The resulting compression force is $N_{cf} = N_p = \frac{A_p f_{yp}}{\gamma_{ap}}$

Distance from top to neutral axis $x_{pl} = \frac{N_{cf}}{b(0.85 f_{ck}/\gamma_c}$ (Eq. 5.4)[4]

The lever arm z is then: $z = d_p - 0.5x$ (Eq. 5.5)[4]

Finally the design resistance moment is equal to: $M_{pRd} = N_{cf}(d_p - 0.5x)$ (Eq. 5.6)[4]

Plastic neutral axis in steel sheeting

The force N_{cf} is now less than N_p. For simplicity, the compression within ribs is neglected and a part of the steel sheeting section is in compression to maintain the equilibrium of the section.

There is no simple method of calculating the distance from top of the depth to the neutral axis, due to the complex properties of profiled sheeting. For this reason the stress distribution is divided into two parts, each diagram represents one part of the design resistant moment $M_{c.Rd}$ as it is shown in Figure 20.

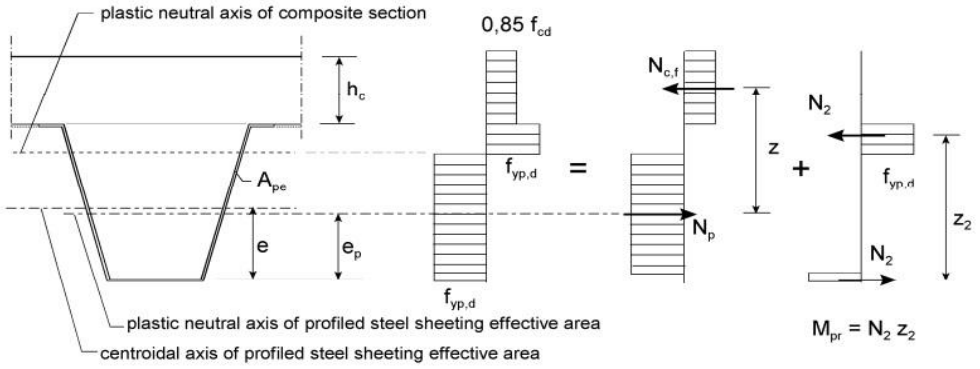

Figure 20 Stress distribution for sagging bending if the neutral axis is inside the steel sheet[7]

• The first diagram represents force $N_{c,f}$ in equilibrium, equivalent to the resistance of the concrete slab part (depth h_c) equilibrated by a partial tension force N_p situated in the steel sheeting.

The distance between mentioned forces is called lever arm z which directly depends on the geometrical characteristics steel profile and its approximate calculation is explained below. The corresponding moment related to this diagram is $N_{cf} \cdot z$

• The second diagram corresponds to a pair of equilibrating forces in the steel profile. In this case the reduced plastic moment of the steel sheeting M_{pr}, is added to the pair achieved by $N_{cf} \cdot z$.

The bending resistance is $M_{pl,Rd} = N_p z + M_{pr}$ (Eq. 5.7)[4]

The compression force in concrete is as equation 5.2: $N_{cf} = 0.85 f_{cd} b h_c$

In Eurocode 4 an approximate method, calibrated by 8 different tests is used with the aim to achieve the expression of the reduced plastic moment resistance of the steel sheeting, M_{pr}. Which can be deduced from M_{pa}.

$$M_{pr} = 1{,}25 M_{pa}\left(1 - \frac{N_{cf}}{A_{pe} f_{yp,d}}\right) \leq M_{pa}$$ (Eq. 5.8)[4]

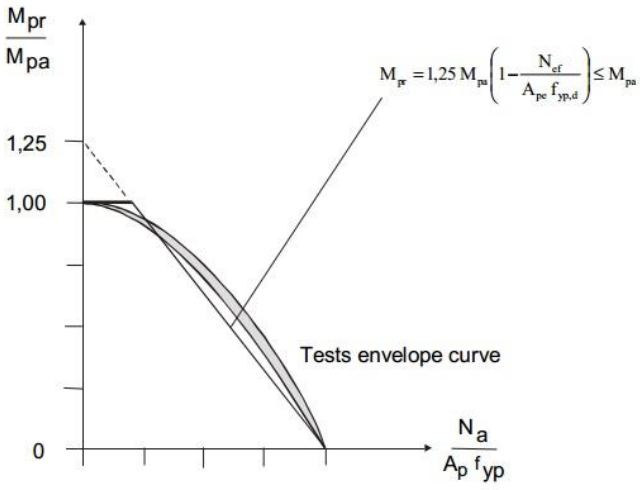

Figure 21 Experimental relation between M_{pa} and M_{pr}[17]

The expression of lever arm is: $z = h - 0.5 h_c - e_p + (e_p - e)\frac{N_{cf}}{A_{pe} f_{yp,d}}$ (Eq. 5.9)[4]

The equal and opposite forces N_{ac} provide a resistance moment M_{pr} equal to the resistance moment for the sheeting, M_{pa}, reduced by the effect of the axial force Na. It should be noted that in Eurocode 4; Part 1.1[4], the value of the symbol N_{cf} depends on the ratio x/h_c. It is the lesser of the two value given by previous equations.

5.4.2. Resistance of composite slabs to longitudinal shear

Type II failure is failure due to longitudinal shear. The aim of this method is to compare the average longitudinal shear resistance τ_u on shear span with the applied force.

To design the slab resistance against the longitudinal shear can be determined by the semi-empirical m-k method or the partial shear connection method.

m-k method

This method uses the full-scale test results to establish the longitudinal shear capacity of the composite slabs. The linear parametric equation used in the semi-experimental m-k method, is composed by most significant resistant parameters present in composite slabs:

$$V_{lR} = F(L_s, d_p, b, A_p, V_t)$$

Where:

V_{lR} longitudinal shear resistance

V_t vertical shear force

d_p average depth of composite slab

3 different tests are done with different L_s longitudes and next graph is built:

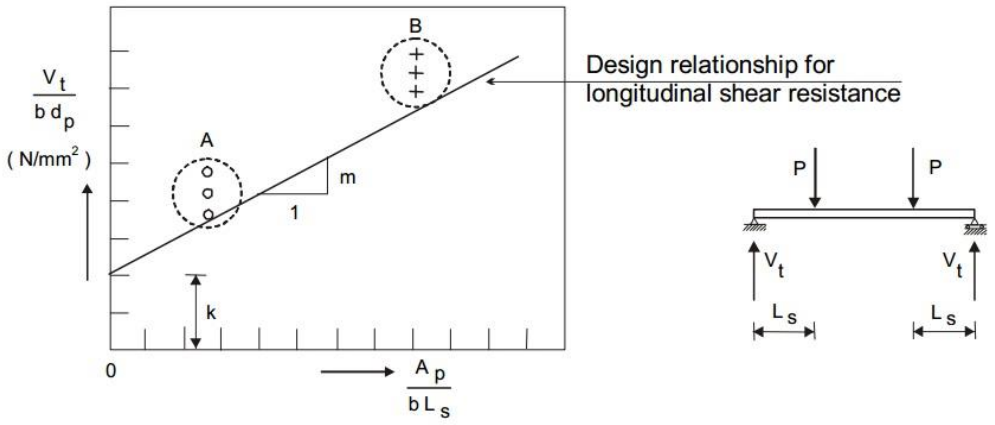

Figure 22 m-k interaction diagram [1]

Where is obtained m-k values

According to Eurocodi-4 the longitudinal shear resistance is given by the expression:

$$V_{l,Rd} = bd_p\left[\left(\frac{mA_p}{bL_s}\right) + k\right]/\gamma_{vs} \qquad \text{(Eq. 5.10)[4]}$$

Where the dimensions are in mm and the partial safety factor for shear connection $\gamma_{vs} = 1.25$

Partial connection method

This method is only used for ductile behavior composite slabs. It is based on the medium value of the design ultimate shear stress $\tau_{u,Rd}$ between steel and concrete interface, on the bending resistance moment from standardized test results and finally on the theoretical partial interaction diagram from ultimate states limits.

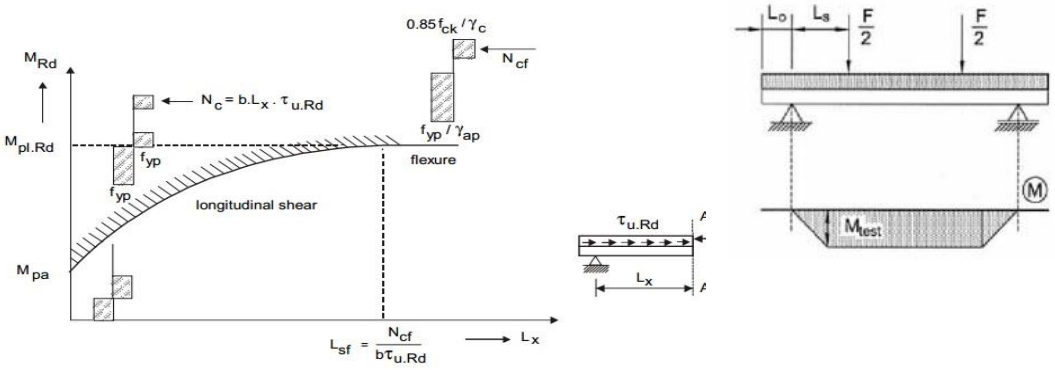

Figure 23 PSC diagram [1].

Where finally the medium shear stress is calculated by next expression:

$$\tau_u = \frac{\eta N_{cf}}{b(L_s+L_0)} \qquad \text{(Eq. 5.11)[4]}$$

This medium value of ultimate shear stress is used to determinate the design ultimate plastic resistance moment for each checking section, for any distance Lx from the support.

5.4.3. Resistance of composite slabs to vertical shear

Failure due to vertical shear has been explained in previous section, noticed as a failure type III. The general formula to calculate the vertical shear resistance $V_{Rd,c}$ has the reinforcement ratio as a part of it, under the precondition that the reinforcement is fully anchored. Nevertheless, the minimum shear resistance formula will be sufficient calculated without considering the commented reinforcement ratio, by:

$$V_{Rd,c} = v_{min} b_w d \qquad \text{(Eq. 5.12) [4]}$$

Where :

$$v_{min} = 0.035 k^{\frac{3}{2}} f_{ck}^{\frac{1}{2}}$$

$$k = 1 + \left(\frac{200}{d}\right)^{1/2}$$

b_w is the minimum width of the cross section in the tensile area

d is the effective depth of the cross section, d ~ d_p for sagging moment

6. Experimental program

In order to carry out this study, 6 different slabs were designed and tested thoroughly. All tests took place at LERMA in the Universitat Politecnica de Catalunya[2][3].

As the maximum capable shear-bond force will be an inherent property for each specific composite slab due to the different interlock mechanism, because the steel profile and the concrete are the same. Four of the six slab tests were produced by the Cofraplus60 (C60) profile by ArcelorMittal, three of them rolled in most usually conventional galvanized steel, and one of them rolled in ferritic stainless steel 1.4003 alloy.

The rest of tests have been obtained with a particular non-embossed profile equivalent to Cofraplus60 without longitudinal stiffeners, where manually by means of folding press, are being implemented all new connection system. The developed tasks are the following:

-Construction and test of 3 slabs using ferritic stainless steel sheeting and common embossments as a connection system: span length of 2600 mm and 100 mm slab depth.

-Construction and test of 1 slabs using galvanized steel sheeting and common embossments as a connection system: span length of 2600 mm and 100 mm slab depth

-Construction and test of 2 different slabs, one of them with the full high density punching connection system, and the other one with the staggered low density punching connection system. Both with 2600mm of span length and 100 mm slab depth.

Specimen code	**Test type**
C60-Inox-2600-100-nº1	*Static*
C60-Inox-2600-100-nº2	*Cyclic + static*
C60-Inox-2600-100-nº3	*Cyclic + static*
C60-CSteel-2600-100	*Static*
PATupc-HI-2600-100	*Static*
PATupc-LO-2600-100	*Static*

Table 3 Type tests

6.1. Type test

There are two different type of test, static tests and cyclic test. Nevertheless, before doing any cyclic test, it must be firstly done one static test, where the load is applied incrementally until reaching to slab breakdown, with the aim of knowing the failure load W_t. As it happens in C60-Inox-2600-100 tests.

- Cylic tests, where the load applied varies between 0.2 W_t and 0.6 W_t, ensure to remove any kind of chemical bond formed between concrete and steel, and the posterior static load test will provide the correct designation of the mechanical bond formed by the embossment. This load may be applied over 5000 cycles in time of at least 3 hours.
- In static tests the load is applied incrementally. Failure load can not occur in less than 1 h.

6.2. Steel sheeting on composite slabs tested

The decision of taking COFRAPLUS 60 as proof tester is due its geometrical simplicity that helps to identify easily the geometrical problems that appear.

Figure 24 illustrates the geometric shape of the profiled steel deck with embossments placed opposite on adjacent webs. For testing has been used sheets with 1013 mm width, and a sheet thickness of 0.8 mm.

Also they are protected from corrosion by a zine coating about 0.02mm thick on each face.

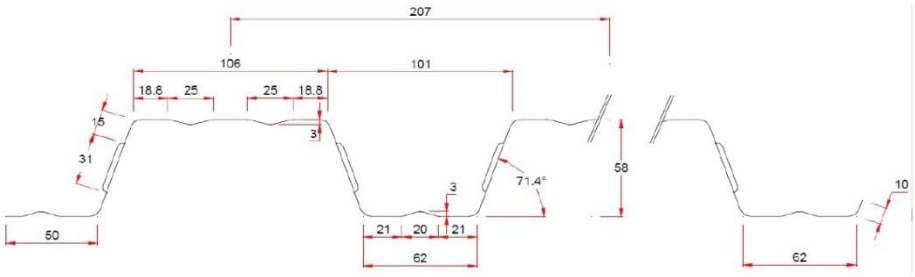

Figure 24 Profile measures

Figure 25 Breakages in steel sheeting.

Figure 26 Shoring before concrete pouring.

Next table summarizes the geometrical properties of all the steel sheets used during tests.

Ferritic stainless steel sheeting					***Galvanized steel sheeting***			
Slab width	b	*1013*	*mm*		*Slab width*	b	*1013*	*mm*
Sheet thickness	t	*0,8*	*mm*		*Sheet thickness*	t	*0,76*	*mm*
Profile length	L_e	*1138*	*mm*		*Profile length*	L_e	*1138*	*mm*
Effective Area	A_p	*910*	*mm²*		*Effective Area*	A_p	*865*	*mm²*
Neutral axis	e	*33,25*	*mm*		*Neutral axis*	e	*33,25*	*mm*
Sheet moment	M_{pa}	*5,71*	*kN·m*		*Sheet moment*	M_{pa}	*5,30*	*kN·m*
Sheet high	e_p	*58*	*mm*		*Sheet high*	e_p	*58*	*mm*

Table 4 Geometrical properties

With regard to material properties, may be assumed elastic properties to be as for structural steel. In accordance to standards EN 1993-1-4 [5], may be obtained steel yield stress, and ultimate resistance of the steel, however, three different cold formed ferritic stainless steel sheets were proved in order to obtain material properties of the composite slabs sheets. The tests were only done in longitudinal direction because it was the only way to obtain a standardized coupon.

No.	Specimen	b mm	t mm	Zn mm	L_o mm	L_f mm	L %	Fu N	$F_{y(0,2\%}$ N	f_u N/mm^2	$f_{y\ (0,2\%)}$ N/mm^2	Date
1	FSS_Sheet	15,98	0,83	0,00	50	63	26	6371	4492	480	339	28-6-11
2	FSS_Sheet	16,12	0,81	0,00	50	64	28	6426	4185	492	321	28-6-11
3	FSS_Sheet	16,08	0,84	0,00	50	64	28	6478	4378	480	324	28-6-11

Table 5 Summarize of the results of the tensile test performed at UPC

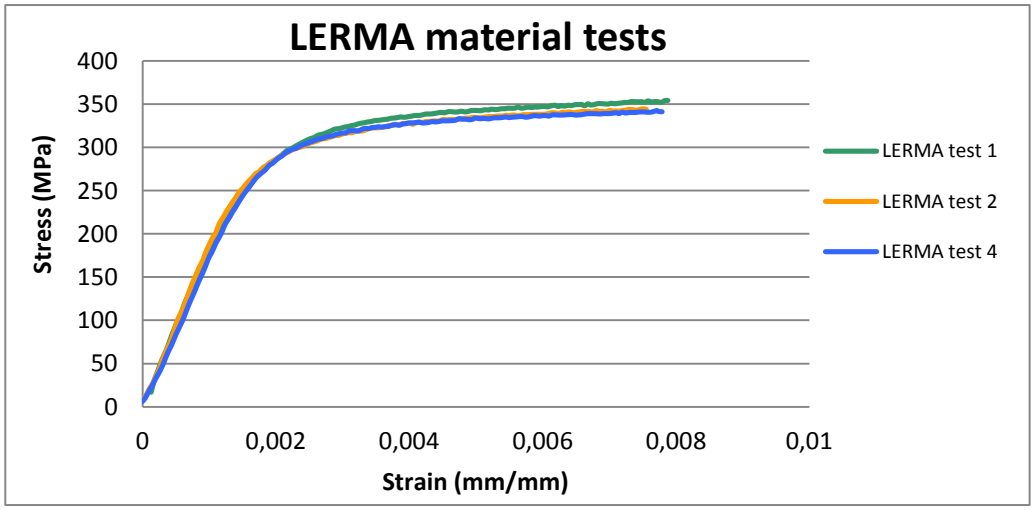

Figure 27 Stress-strain curves of the tensile test performed by UPC

Table 5 is finally summarizing both the stainless and galvanized steel yield stress. Ferritic stainless steel sheeting obtained from tensile tests on strips taken from the profiled sheeting, and galvanized steel properties from standards EN 1993-1-4 [5].

	***Yield Stress* [N/mm²]**	***Young´s modulus* E [N/mm²]**
Ferritic Stainless Steel	*326*	*218.000*
Galvanized Carbon Steel	*350*	*210.000*

Table 6 Steel yield stress

6.3. Concrete testing

Concrete used on slab testing has been C25/30 and must follow the specifications of EN-1992-1-1 [6], where are indicated the process to obtain the characteristic strength of concrete. The test of the concrete will be determined after 28 days doing compressing test with standard cylindrical concrete specimens of 150 mm diameter and 300 mm height. There must follow the specifications of UNE EN 12390-3 [11]. To carry out the compression testing, after disassembly from moulds must be regularized top and bottom of the specimens. The speed of the process is 8,85 kN/s and from each specimen is obtained the maximum force database, the cylinder compressive strength of concrete and the maximum distance of the mechanism between the beginning and the end of the process.

Specim.	**Day of concreting**	**Day of testing**	**Type test**	**Speed (kN/s)**	**Maximum force (kN)**	**Maximum distance(mm)**	**Compressive strength (MPa)**
1	10-ene-13	27-feb-13	Compression	8,8537	586,6	1,42	33,2
2	10-ene-13	27-feb-13	Compression	8,8537	601,1	1,41	34,01
3	10-ene-13	27-feb-13	Compression	8,8537	597,9	1,36	33,83
4	10-ene-13	27-feb-13	Compression	8,8537	588	1,37	33,27
5	10-ene-13	26/04/2013	Compression	8,8537	679,7	2,82	38,46
6	10-ene-13	26/04/2013	Compression	8,8537	690,9	1,75	39,1
7	10-ene-13	26/04/2013	Compression	8,8537	674,4	1,95	38,16
8	10-ene-13	26/04/2013	Compression	8,8537	705,8	1,78	39,94

Table 7 Testing process and concrete properties(truck 2)

Two different concrete trucks were tested to carry out the process. The previous table shows the values acquired with the truck number 2. As it is observed the specimen lot with 106 days has a higher strength property compared with the specimen lot of 48 days. To sum up the concrete testing resumes that including both trucks, the compressive cylinder strength of concrete (106 days) is 39,81 Mpa and compressive cylinder strength of concrete (48 days) is 33,58 Mpa.

6.4. Test set-up

The tests have been carried out following the procedure described in Eurocode4 to obtain the longitudinal shear resistance by m-k parameters in traditional embossments, and to obtain the behavior of the new connection system in composite slabs. In figure 27 is shown the schematic view of arrangement for the simply supported composite slab, all of them were single-span and monotonically loaded, configuration with an effective span (L) of 2.6 m and subjected to two symmetrically located uniformly distributed line loads, applied on two HEB beams.

Loading was applied by a single hydraulic jack system, where the load was applied by increments.

Moreover there was mounted one structural spreader beam bellow to the structural load beams, placed back to back, and load is measured with the help of cell at the point of application. Uniform loading is applied by stiff and flexible 100mm width neoprene pads over a levelling sand layer, aim for a uniformly distributed load. Two steel plates with two greased Teflon sheets between them were used, under neoprene, to eliminate the lateral confinement produced by friction between the slab and the testing machine.

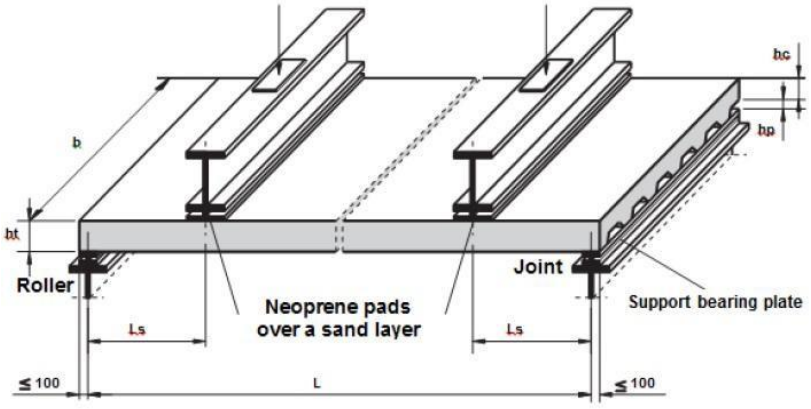

Figure 28 Test slab[20]

One support is a fixed joint and the other one is a rotating roller. This arrangement achieves a constant bending moment and pure bending in the central zone of the composite slab. The shear force is constant between the load application and support cross-sections

Roller and hinge supports are specially fabricated for study. The schematic view of the roller and hinge supports is shown in Figure 28.

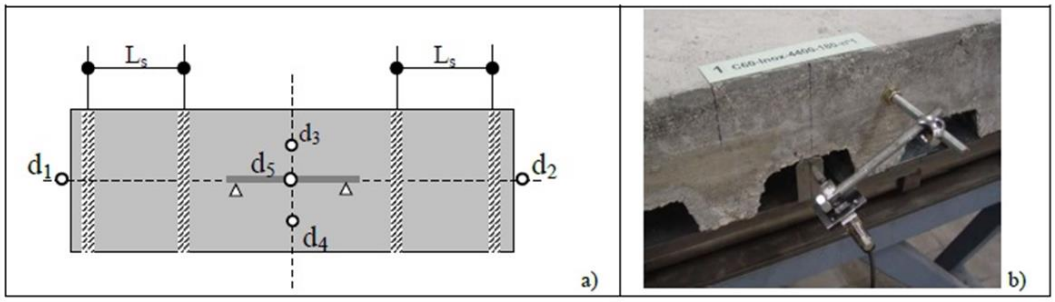

Figure 29 Displacement sensors on testing.

Linear displacement sensors are measuring the deflection at the middle of the span (d3 and d4). Furthermore, there are two other sensors fixed to the concrete at each end of the slab measuring the relative slip of the steel and the displacement of the slabs (d1and d2). The sensor d5 is incorporated to a central curvature meter, and its intention is measure the deflection which permits to obtain the curvature radius.

7. Test results and slabs behavior

Initially it carried out static a test in order to know the loading range which may be applied on dynamic tests (C60-Inox-2600-100-nº2,3). To determine the maximum load supported in a slab, it may be added to the maximum cell force applied in test, the self slab weight and the beams weight. The sum of three forces is obtained the maximum load which produced the breakdown on the composite slabs W_t.

Next table collects the theoretical maximum loads which have produced the slab breakdown.

Specimen code	F_{max} (kN)	$Slab\ weight(kN)$	Beams weight(kN)	$W_t(kN)$	$V_{max}(kN)$	$M_{max}(kN \cdot m)$
C60-Inox-2600-100-nº1	35,05	3,95	0,47	39,47	19,74	12,82
C60-Inox-2600-100-nº2	39,51	3,95	0,47	43,93	21,97	14,27
C60-Inox-2600-100-nº3	36,24	3,95	0,47	40,66	20,33	13,21
C60-CSteel-2600-100	36,06	3,95	0,47	40,48	20,24	13,16
PATupc-HI-2600-100	83,08	3,95	0,47	87,50	43,75	28,44
PATupc-LO-2600-100	90,74	3,95	0,47	95,16	47,58	30,93

Table 8 Efforts on composite slabs[2]

Specimen code	$0.2 \cdot W_t(kN)$	$0.6 \cdot W_t(kN)$	$Minimum\ force$	$Maximum\ force$
C60-Inox-2600-100-nº2,3	*7,89*	*23,68*	*3,47*	*19,26*

Table 9 Dynamic test loads [2]

M_{max} and V_{max} have been calculated supposing it is applied a load called P subjected to two symmetrically located uniformly distributed line loads, as it is loaded in tested case, then theoretical effort moments on the slabs have been studied.

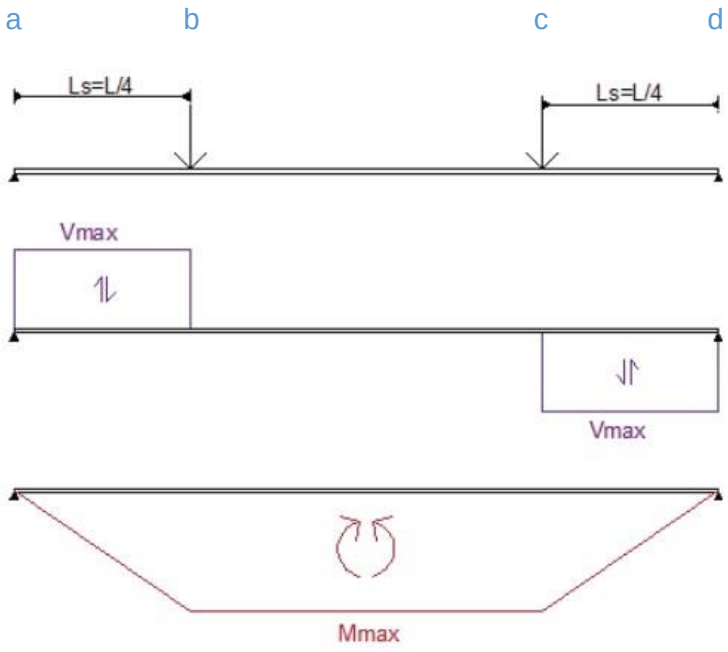

Figure 30 Effort distribution

Moment distribution for each part is:

$$M_{ab} = F \cdot x = \frac{P}{2} \cdot x$$

$$M_{bc} = P \cdot \frac{L}{4} = \frac{P}{2} \cdot \frac{L}{4} = \frac{PL}{8}$$

$$M_{cd} = P(L - x)$$

The resulting maximum moment available in the slab is $\boldsymbol{M_{max} = \frac{PL}{8}}$ .and shear force is $\boldsymbol{V_{max} = P/2}$.

From table 7 is obtained the medium shear effort capable to support which is 20,57 N for the group of composite slabs which use the common embossments, meanwhile the result is 46,13 N for the group of slabs with the new patent connection.

The resulting moment is also different between groups, the traditional composite slabs have a medium moment of 13,36 kN·m and the new composite slabs 29,68 kN·m, which clearly shows more than double difference between each group.

Next *Table 9* summarizes the results in terms of resultant forces, midspan deflection and slip about all tests completed. $F_{0.1\,mm\,slip}$ and $F_{0.5\,mm\,slip}$ show the forces where the slip, measured by displacement sensors number one and two, has a measure of 0.1 mm and 0.5 mm respectively. Such information is going to be useful in order to know the ductile or brittle behavior of the slab. Then F_{max} shows the maximum force capable to be loaded for the composite slab. In addition to this the measurements about the midspan deflection and the slip were picked up at the force which was produced the slab breakdown.

	Load cell force				***Displacement at F_{max}***	
Specimen code	$F_{0.1\,mm\,slip}$ (kN)	$F_{0.5\,mm\,slip}$ (kN)	F_{max} (kN)	$F_{\frac{L}{50}}$ (kN)	$\delta_{Midspan}$ (mm)	$Slip\ (mm)$
C60-Inox-2600-100-nº1	3,61	9,77	35,05	34,50	52,55	5,68
C60-Inox-2600-100-nº2	3,52	9,92	39,51	36,67	70,77	5,46
C60-Inox-2600-100-nº3	4,37	7,95	36,24	34,86	66,77	6,37
C60-CSteel-2600-100	23,47	20,00	34,15	34,15	75.22	4,69
PATupc-HI-2600-100	**No slip**	**No slip**	**83,08**	**69,35**	**> 90**	**No slip**
PATupc-LO-2600-100	**No slip**	**No slip**	**90,74**	**75,04**	**> 120**	**No slip**

Table 10 Slabs behavior[2]

As it shows in the table, the first noteworthy fact, which only reaffirms the suppositions made before about the new patent UPC connection system behavior, is the inexistence of any slippage between materials in the slabs where have been applied the commented mechanism. Secondly, there is a big difference in the ultimate force and the midspan deflection capable to service between the slabs with traditional embossments and the

composite slabs with the patent connection system.

In cyclic test the midspan deflection displacement in the maximum force for slab tests number 2 and 3 was 10.62 mm and 11.10 mm respectively, meanwhile the slip at the maximum force is 0.98 mm and 1.46 mm.

In following sections will be explained and commented in detail all differences between composite slabs behavior.

7.1. Midspan deflection and slippage

Firstly, in figures 31 and 32 are graphed the load cell force versus midspan deflection and longitudinal slip in only slabs with common embossments system behavior, comparing the differences between ferritic stainless steel and galvanized steel.

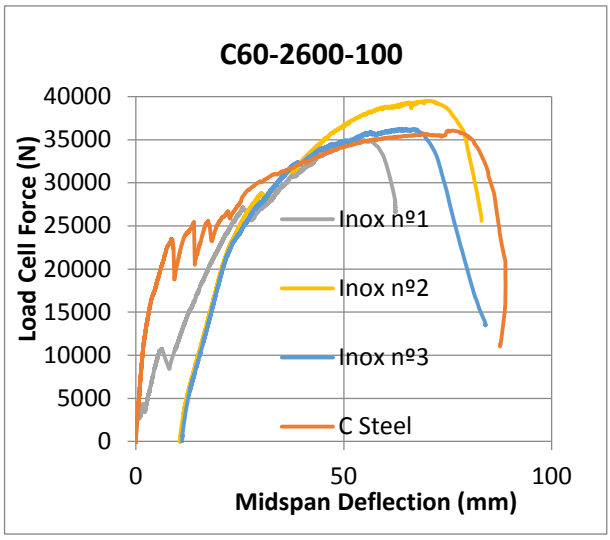

Figure 31 Load cell force vs midspan deflection

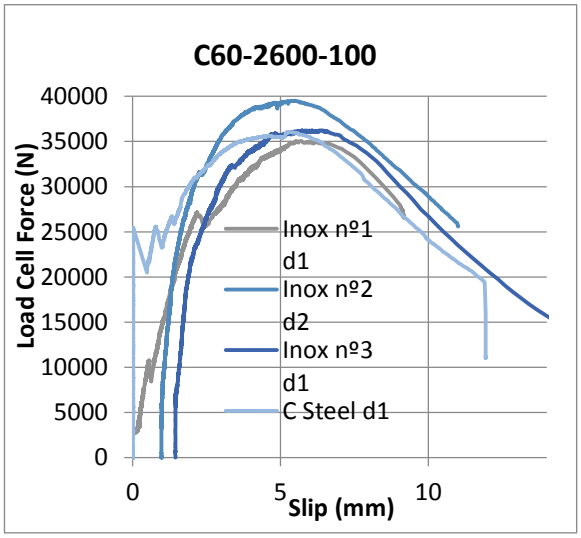

Figure 32 Load cell force vs slippage

All of them have a parabolic deformation instead of linear deformation, additionally the use of ferritic stainless steel or conventional carbon steel as steel sheeting, has no effect in terms of resistance values and they have similar initial slope, due to the similarities in Young's modulus and the yield stresses. As it was explained in previous section the tested slabs 2 and 3 preceded to static test they had a cyclic test. Each figure shows the midspan deflection and the slippage in static test.

For this reason both slabs start their static test, after any load applied, with the maximum midspan deflection displacement achieved in cyclic test (10.62 mm and 11.10 mm respectively), and the slip achieved during the cyclic test of 0.98 mm and 1.46 mm.

Another interesting point is the abrupt curve drop off, once the slab reaches the ultimate load and then the slab is collapsed.

Regarding to load where the first slippage was produced, there are big differences between materials used. Focusing on the load where is produced 0,5 mm of slippage, the election of galvanized steel as a surface sheeting caused higher resistance values than for stainless steel speciments (Fig 32). The weaker initial adherence is probably because the overly smoother surface of stainless steel due to different chemical reaction of the concrete on stainless steel or zinc surfaces.

Moreover peaks observed in both figures are the instants where the loss of side slip adhesion between concrete and steel had occurred, which as a result, midspan deflection increased without a load application. It is also observed that in tests which have previously supported cyclic loading, the chemical bond is destroyed only remaining mechanical attachment. Therefore in the midspan deflection graph are observed less "peaks" due to the no adhesion breakage do not occur.

In order to understand that phenomenon next figure illustrates the behavior of slab test number one (steel sheet made by ferritic stainless steel sheeting and common embossments curves), where are compared displacement sensors d1 and d2, which also illustrates the existence of slippage, with midspan deflection of the same slab.

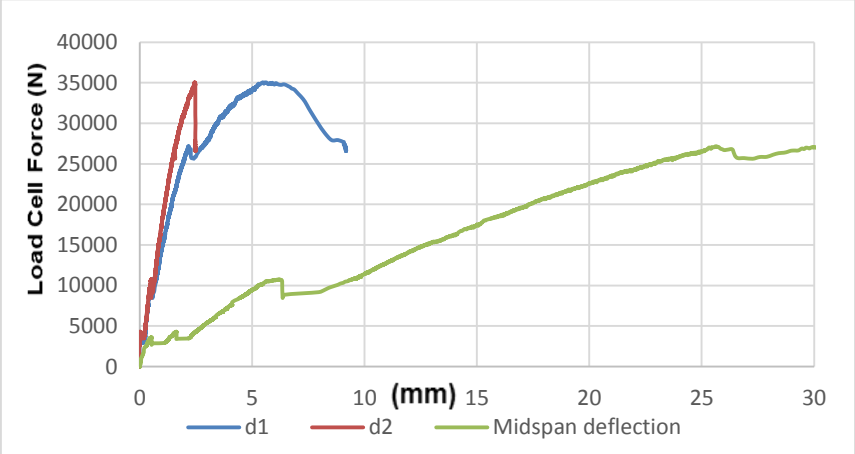

Figure 33 Picks comparison

The previous figure shows how at the beginning the load increases without slipping and producing a very small midspan deflection until reaching 6000 N when the first slipagge in one side occurs. At this moment the midspan deflection without application of load increases.

After increasing the load, the slippage occurs on the other side, which consequently the midspan deflection considerably increase. This phenomenon is observed until to reach the collapse of the structure where is observed how the increase of the midspan deflection while two courves d1 and d2 remain constant. In this figure is shown the influence of the slippage over the midspan deflection and the direct relationship they have.

Now, it is added to the previous figure the curves of slabs with the new connection system.

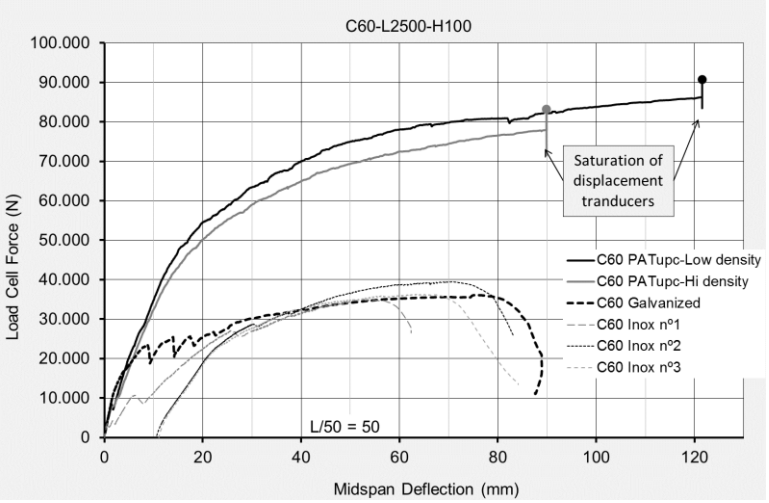

Figure 34 Midspan deflection

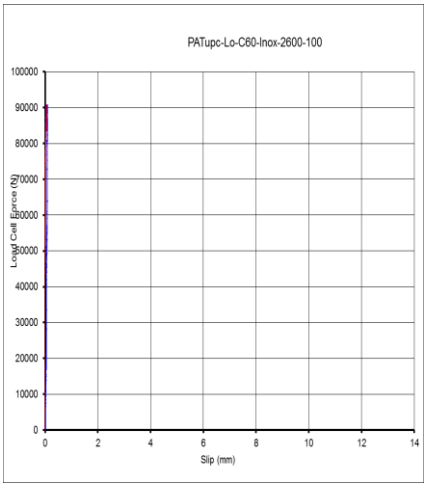

Figure 35 Slippage

Figure 35, shows the inexistence of .any slippage on new composite slabs and clearly represents how the new connection system keeps full connection up to failure because no slippage curve is shown in figure. In addition to this, in figure 34 is demonstrated how maximum deflection, which was only limited by the extension capability of the hydraulic cylinder, of new composite slab are much higher than the slabs with traditional embossments. Also it is observed the fact that the maximum load capable to reached, before the decreasing branch was developed, is widely higher in new composite slabs as it was proved in table 10.

7.2. Cracking

During the slab tests, it was tested that as much increased the load, before any visible cracks in all concrete slabs, a slight cracking between the steel sheeting and concrete was heard. This fact is almost similar in all shear spans.

In most cases of slabs with traditional embossments, the first relative end slip were detected at the end of the side when the initial crack was formed, moreover the loading was capable of considerable increase in magnitude before a much louder debonding cracking was heard and more major cracks of concrete were observed, nevertheless instead of that, due to the relative displacement between the steel sheeting and the concrete, and consequently the cracking started to develop upward to the top of the concrete, the premature fail occurred.

However, with the patent connection system by UPC, initial flexural fine cracks were initiated at the bottom of concrete near the load points and subsequently fine cracks developed in the midspan as the loading being sustained, but they had no consequence in debonding slips.

Figure 36 Cracking on slabs

7.3. Stress-strain distribution

To reveal the steel and concrete stresses and differences between shear-bond mechanisms on slabs tested, four strain gauges were monitored on different positions of the steel deck, and one strain gauge was monitored over the slab depth in order to measure stresses of concrete.

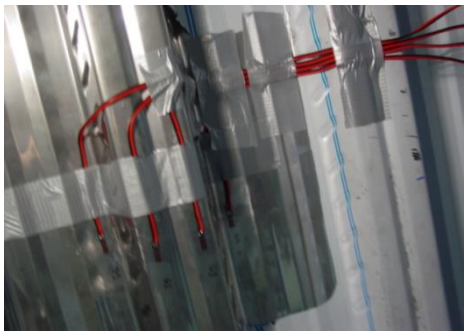

Figure 37 Gauges applied in profile

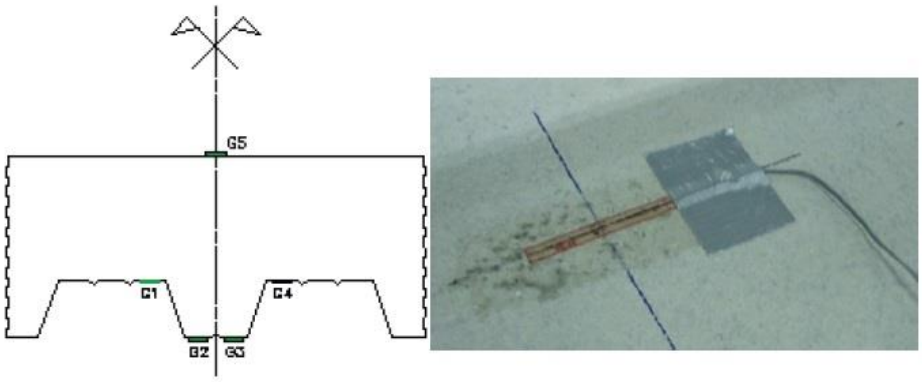

Figure 38 Gauges distribution.

Strain gauges measurements showed that both materials are widely yielded, but it is also observed some differences explained in following subsections.

7.3.1. Ferritic stainless slabs with common embossments

As it is illustrated on figure 39 bottom flanges of the steel deck (g2 and g3) and most of the web of steel sheeting were all subjected to tension stress from the beginning to the ultimate state, meanwhile the top flanges of the steel deck (g1 and g4) changed from being stressed in tension, prior to initial slip between the concrete and the steel sheet to being stressed fully in compression at the ultimate state in the all specimens. The mentioned change with stresses tensioned to compressed occurs approximately at 10 kN load. The reason of this fact is aside of slippage between materials, the concrete cracking.

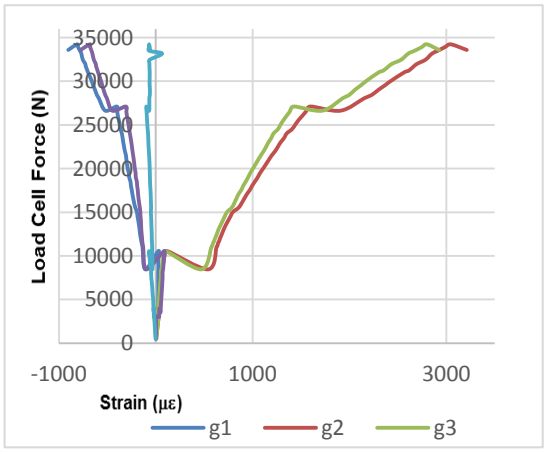

Figure 39 Strain measures

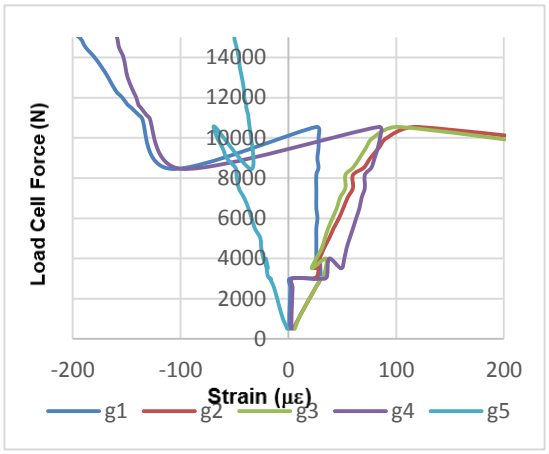

Figure 40 Focused strain measures

From gauge 5 it is shown concrete portion was in tension during the test, but also illustrate that there were rapid strain increases in concrete before cracks initiated at a load of 11.8 kN.

Figures 41 and 42 illustrate how varies the curves of deformations compared with the measurement to achieve the curvature by displacement sensor d5, and it is shown how concrete measured by gauge g5 increases its deformation 0 to -70με with almost no curvature appears.
After this point cracking appears in the concrete and there is no more deformation increase but curvature keeps increasing.

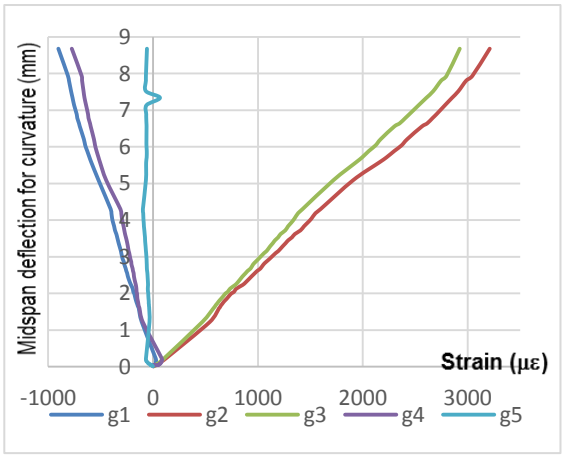

Figure 41 Strain measures(d_5)

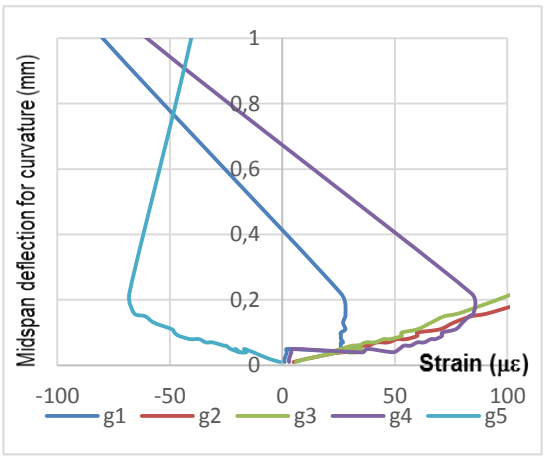

Figure 42 Focused strain measures(d_5)

As it is also shown in figure 41, the deformation applied on the bottom flanges of the steel deck (g2 and g3) is directly proportional to midspan deflection in the slab.

7.3.1. Galvanized slabs with common embossments

From the curves of strains varying with the exerted load, here it is illustrated that the state where top flanges of the steel profile (g1 and g4) turn into compression due to the localized separation at the interface occurs in a much higher load than in ferritic stainless slabs. Almost considered as a ultimate failure state
Nevertheless the bottom flange and most of the web of steel sheeting are still in tension.

Local buckling occurs in the top flange and in the major parts of web of steel sheeting, and the bottom flange of steel sheeting stressed in tension reaches its yielding strength

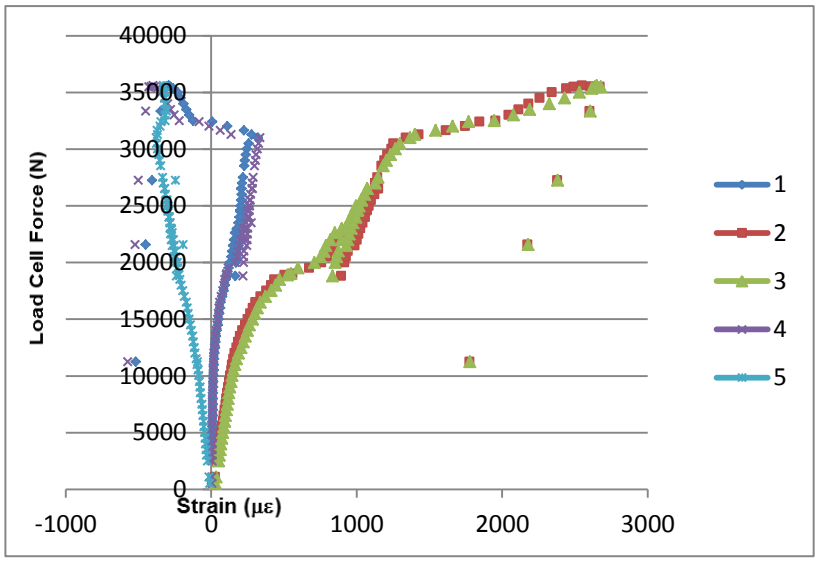

Figure 43 Strain measures in galvanized slabs

7.3.2. Slabs with new connection system

Figure 44 perfectly illustrates how the ultimate values were reached without slipping at all, similar strain increases in the bottom of steel deck as well as on top of the concrete were also detected when cracks initiated, when a force of 45000N was loaded on the slab. Nevertheless gauges g1 and g4 are subjected to tension stress from the beginning to the ultimate state due to no slippage occurs.

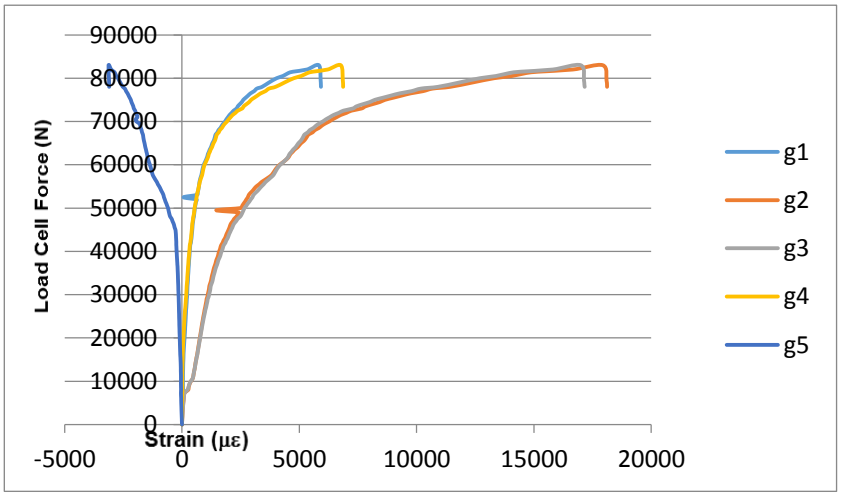

Figure 44 Strain measures in new composite slabs

In order to check the strain-stress diagram where for each point stress, there might be same strain, as a consequence, after the load increased the proportion between gauges position distance need to be similar. A scale magnification was created in figure, where a depth slab web simulation was formed to check the mentioned proportion.

It is shown how at the beginning of the test, before any possible cracking, the proportion between the distance of each gauge situated on the web of the slab is exact, but after loads louder than 10kN exactly proportion does not exactly remain.

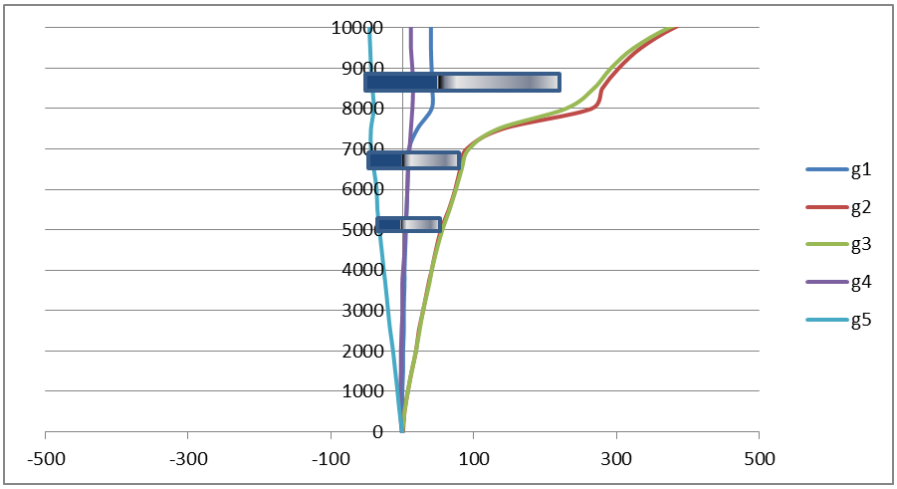

Figure 45 Strain measures proportion in new composite slabs

8. Ultimate limit state service

Before starting to calculate the ultimate state service in the different slabs tested, it is worth nothing that the effective area A_{pe} of the steel decking, for each calculation, is the net section obtained without considering the galvanising thickness (generally 2 x 0,020 = 0,04 mm).

Moreover, the width of embossments, indentations and all crown-shaped breakages generated in the steel sheet are also neglected, unless it can be proved by tests that there is a lager effective area.

For these reasons, the effective area per metre width, A_p, and the height of the center area above the bottom of the sheet, e, are usually based on tests. These usually also show that ep, is different from e.

In this section is going to study in theoretical way the ultimate state service and it will be compared with the tested experiments on different slabs.

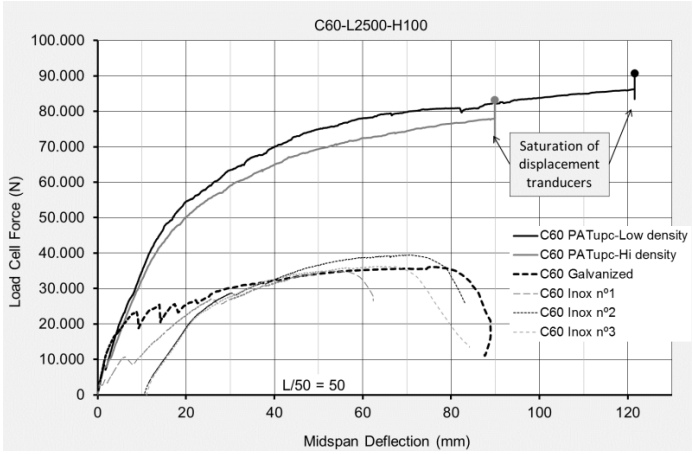

Figure 46 Ultimate experimental force service

8.1. Ultimate limit state in new connection system slabs

As it is shown in figure 46 the ultimate limit force capable to reach in new composite slabs is in the order of 80 to 90 kN. So the applying the equation before demonstrated $M_{max} = \frac{PL}{8}$ of ultimate bending moment which corresponds to the plastic bending moment of the composite cross section, should be achieved a theoretical maximum load around the order of 80kN.

As it was explained in section 5.4.1, when there is full connection between concrete and steel, as it is considered the slabs with the new connection patent, it is firstly compared N_{cf} and N_p in order to know where the neutral axis is situated.

All characteristics material dates of composite slabs with new patent system as a connection mode, are shown in next table.

Concrete or Steel	***Value***	***Units***
αf_{cd}	33,58	N/mm^2
f_{yb}	326	N/mm^2
f_{yu}	480	N/mm^2

Table 11 Materials characteristics.

Applying formulas 5.2 and 5.3:

$$N_{cf} = \alpha f_{cd} b h_c = 33.58 \cdot 1013 \cdot 42 = \mathbf{1428,69\ KN}$$

$$N_p = A_p f_{yb} = 910 \cdot 326 = \mathbf{296,79\ KN}$$

In studied case $N_{cf} > N_p$, so the neutral axis is situated above the sheeting, therefore there must be applied all formulas also explained in section 5.4.1, in order to achieve the design resistance moment. After applied all dates of table is showed above.

$$N_{cf} = N_{pa} = \frac{A_p f_{yp}}{\gamma_{ap}} = 910 \cdot 326 = 29660N$$

$$x_{pl} = \frac{N_{cf}}{b(0.85 f_{ck}/\gamma_c} = \frac{29660}{1080 \cdot 33.58} = 8{,}72mm$$

$$M_{p,Rd} = 910 * 326 * \left(67 - 0.5 * \frac{910*326}{1013*33{,}58}\right) : \mathbf{18582,62}KNmm$$

$$M_{max} = \frac{PL}{8} = M_{p,Rd} = \mathbf{18582,62KNmm}$$

Theoretical P_{max} = **57177 N**

As it has been tested and exposed in section 7, the real ultimate resistance force in new composite slabs is higher than the theoretical P_{max} previously calculated. The reason is because the steel stress on calculations is lower than the stress which is the steel capable to reach.

For this reason is recalculated the ultimate plastic bending moment in order to achieve the ultimate force to service in composite slab using the same procedure exposed previously but in this case using the maximum yield stress of steel $f_{yu.}$

It is firstly compared :

$$N_{cf} = \alpha f_{cd} b h_c = 33.58 \cdot 1013 \cdot 42 = \mathbf{1428,69\ KN}$$

$$N_p = A_p f_{yb} = 910 \cdot 480 = \mathbf{436,80\ KN}$$

In this case as it happened before $N_{cf} > N_p$, so the neutral axis is situated above the sheeting.

$$N_{cf} = N_{pa} = \frac{A_p f_{yp}}{\gamma_{ap}} = 910 \cdot 480 = 436800N$$

$$x_{pl} = \frac{N_{cf}}{b(0.85 f_{ck}/\gamma_c} = \frac{29660}{1080 \cdot 33.58} = 12{,}84\ mm$$

$$M_{p,Rd} = 910 * 326 * \left(67 - 0.5 * \frac{910*326}{1013*33{,}58}\right) : \mathbf{26461,17} KNmm$$

$$M_{max} = \frac{PL}{8} = M_{p,Rd} = \mathbf{26461,47 KNmm}$$

Theoretical P_{max} = **81418 N**

Which result is much closer to the real ultimate state service in composite slabs with new connection system.

8.2. Ultimate state service in slabs with traditional embossments as connection system

The failure mode in composite slabs which have used the traditional embossments, as it proved the test data, has been due to longitudinal shear. As it was previously commented there are two ways to achieve the average longitudinal shear resistance τu on shear span L_s and compare this with the applied force. In this case is going to use the partial interaction design method.

Before starting to calculate anything, as it guides the EN-1994-1-1 [4] section 9.7.3, there must be proved how is the slab breakdown, ductile or brittle. Because if it is ductile it is taken V_t as a half of the breakdown load W_t, otherwise the value V_t must be reduced using the factor 0.8.

- The longitudinal shear behaviour may be considered as ductile if the failure load exceeds the load causing a recorded end slip of 0,1 mm by more than 10%.
- If the maximum load is reached at a midspan deflection exceeding L/50, the failure load should be taken as the load at the midspan deflection of L/50.

The W_t is the sum of ultimate force, slab weight and beams weight. It is calculated in order to find the load where the midspan deflection of L/50 and the load which causes end slip of 0.1 mm.

Specimen code	$W_t(kN)$	$F_{\frac{L}{50}}$ (kN)	$W_{t(\frac{L}{50}}$ (kN)	$F_{0.1\,mm}$ (kN)	$W_{t\,0.1\,mm}$ (kN)	$W_{t\,0.1\,mm+10\%}$ (kN)	***Ductile*** ***brittle***
C60-Inox-nº1	39,47	34,50	38,92	3,61	8,03	8,83	**Ductile**
C60-Inox-nº2	43,93	36,67	41,09	3,52	7,94	8,73	**Ductile**
C60-Inox-nº3	40,66	34,86	39,28	4,37	8,79	9,67	**Ductile**
C60-CSteel	40,48	34,15	77,86	23,47		30,68	**Ductile**

Table 12 Ductile or brittle behavior[3].

8.2.1. Partial interaction design

The moments acting on the composite slab in the collapse instant, have an intermediate value between the null connection and total connection, so it is necessary to evaluate the degree of connection corresponding for each slab. The value of resistance τ_u depends on the type of sheeting and must be established for all proprietary sheeting as the value is a function of the particular arrangements of embossment or indentation orientation, surface condition etc.

The acting axil force in the concrete when the neutral axis is situated in the steel sheeting, is calculated as in next table.

Equilibrium	$M_{test} = N_c \cdot z + M_{pr}$ (Eq. 8.7)	$N_c = \eta \cdot N_{cf}$ (Eq. 8.1)
		$z = d_p - 0.5 \cdot \eta \cdot X_{cf} - e_p + (e_p - e) \cdot \eta$ (Eq. 8.2)
		$M_{pr} = 1.25 \cdot M_{pa} \cdot (1 - \eta)$ (Eq. 8.3)
	$A \cdot \eta^2 + B \cdot \eta + C = 0$ (Eq. 8.8)	$A = (e_p - e - 0.5 \cdot X_{cf}) \cdot N_{cf}$ (Eq. 8.4)
		$B = (h_t - e_p) \cdot N_{cf} - 1.25 \cdot M_{pa}$ (Eq. 8.5)
		$C = 1.25 \cdot M_{pa} - M_{test}$ (Eq. 8.6)

Table 13 Equilibrium design.

Where M_{pa}, e, e_p h_t, and d_p are characteristics from each steel sheeting, which have been described in table 3. Then η is the degree of shear connection defined as the ratio between the force in the sheeting evaluated from the tests and the forces on the sheeting which causes full yielding, calculated as $\eta = {N_c}/{N_{cf}}$ and N_{cf} is the minimum value between $A_p f_{yb}$ and $\alpha f_{cd} b h_c$.

The last plastic torque $M_{pl,rd}$ is calculated by the multiplication of values N_{cf} and $x_{pl} = \frac{N_{cf}}{b(0.85 f_{ck}/\gamma_c}$.

Specimen code	$\boldsymbol{M}_{\boldsymbol{test}}$ $\boldsymbol{(kN \cdot m)}$	$\boldsymbol{M_{test}/M_{pl,rd}}$	$N_c(kN)$	η
C60-Inox-nº1	10,85	0,586	136,13	0,459
C60-Inox-nº2	12,08	0,652	167,72	0,565
C60-Inox-nº3	11,18	0,604	144,92	0,488
C60-CSteel	11,13	0,642	152,85	0,552

Table 14 Degree of shear connection[3].

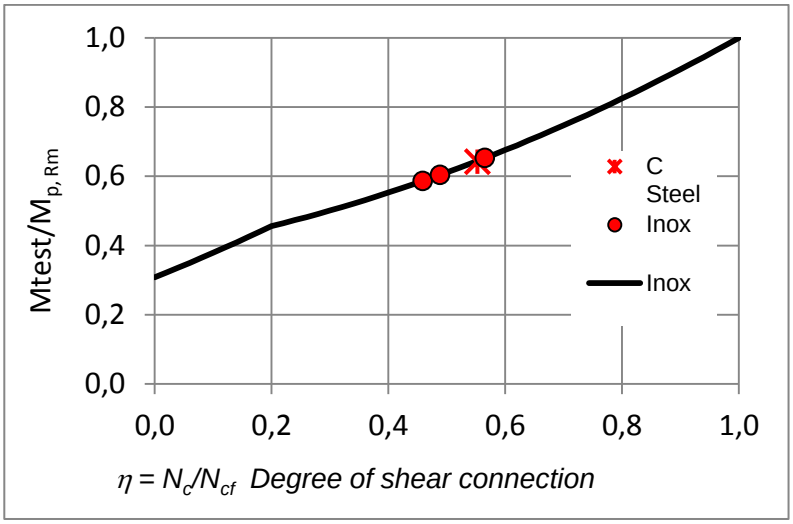

Figure 47 Degree of shear connection.

As it is observed in the figure 46 , the degree of shear connection obtained from the carbon steel specimens is higher than the ferritic stainless steel specimens.

Depending on if the support reaction has been taken into account as a cause of longitudinal shear resistance, there are two different ways to calculate it. The default value of the friction coefficient μ is taken as 0,5.

$$\tau_u = \frac{\eta N_{cf}}{b(L_s+L_0)} \text{ (Eq. 8.9)} \qquad \tau_u = \frac{\eta N_{cf} - \mu V_t}{b(L_s+L_0)} \text{ (Eq. 8.10)}$$

The value of longitudinal shear stress has been obtained applying all information explained before, and is exposed in following tables.

Specimen code	$\tau_u(\frac{N}{mm^2})$	$\tau_{u,m}(\frac{N}{mm^2})$	$\tau_{u,RK}(\frac{N}{mm^2})$	$\tau_{u,Rd}(\frac{N}{mm^2})$
C60-Inox-nº1	0,208	0,229	0,209	0,167
C60-Inox-nº2	0,258			
C60-Inox-nº3	0,222			
C60-CSteel	0,235	-	-	0,188

Table 15 Longitudinal shear resistance taking into account the effect of friction at the supports[3]

Specimen code	$\tau_u(\frac{N}{mm^2})$	$\tau_{u,m}(\frac{N}{mm^2})$	$\tau_{u,RK}(\frac{N}{mm^2})$	$\tau_{u,Rd}(\frac{N}{mm^2})$
C60-Inox-nº1	0,224	0,246	0,225	0,180
C60-Inox-nº2	0,276			
C60-Inox-nº3	0,238			
C60-CSteel	0,251	-	-	0,201

Table 16 Longitudinal shear resistance without the effect of friction at the supports[3]

The characteristic shear strength $\tau_{u,RK}$ has been calculated from the test values as the 5% fractile using an appropriate statistical model in accordance with EN 1990, Annex D[4]. The design shear strength $\tau_{u,Rd}$ is the characteristic strength $\tau_{u,RK}$ divided by the partial safety coefficient γ_{VS} of 1.25.

8.2.2. Differences between steel sheets

Despite the fact that there are some differences on ultimate limit states parameters between stainless-steel and conventional steel sheeting, these are not significant regardless of the calculation method used in past sections. Partial connection method, applied to stainless-steel have achieved a higher ultimate longitudinal shear resistance compared with the medium of tests made by conventional sheeting, nevertheless, the differences are in the order of hundredths, so it might be supposed similar results.

9. Behavior of slabs with new connection system

9.1. Neutral axis behavior in new patent slabs

As it is known the neutral axis is an axis in the cross section of a slab where there are no longitudinal stresses or strains.

All fibers on one side of the neutral axis are in a state of tension, while those on the opposite side are in compression. Therefore by the intermediate value theorem, there must be some point between the top and the bottom of the slab that has no strain, since the strain in a slab is a continuous function.

The bending is considered uniform and pure, therefore there is a distance y from the neutral axis with the inherent property of having no strain and a longitudinal normal strain ε_x varies linearly with the distance y from the neutral surface.

$$\varepsilon_x(y) = \frac{L(y)-L}{L} = \frac{\theta(\rho-y)-\theta\rho}{\theta\rho} = \frac{-y\theta}{\rho\theta} = \frac{-y}{\rho} \qquad \text{(Eq. 9.1)}$$

Where :

L is the original length of the slab (span)

ε(y) is the strain as a function of coordinate on the face of the slab.

σ(y) is the stress as a function of coordinate on the face of the slab.

ρ is the radius of curvature of the slab at its neutral axis.

θ is the web slab angle

9.1.1. Curvature radius of the slab

In order to obtain the radius of curvature, it has been used all measurements obtained by d5 and after trigonometric calculations process it has been developed a formula where only depends on d_5 and a, where a with a measure of 450mm is half of the distance from one of the relative supports to the position on the middle of the slab where is measured d5.

The trigonometric process to achieve the commented equation is explained in following part:

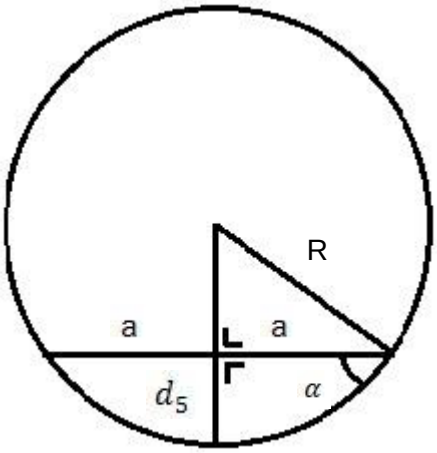

Figure 48 Trigonometric calculations to obtain curvature radius

$$\tan^{-1}\frac{d_5}{a} = \alpha$$

$$\frac{d_5}{a} = \frac{a}{2R - d_5}$$

Finally the resultant equation to obtain the radius of curvature is :

$$R = \rho = \frac{a^2}{2d_5} + \frac{d_5}{2} \qquad \text{(Eq. 9.2)}$$

9.1.2. Comparison between gauge measures and theoretical strains.

In order to achieve the results, it has been studied the experimental strains of a sequence of forces and they have been compared with the theoretical strains calculated by the equation 9.1.

To solve the commented equation is required to suppose the distance from top of depth slab to neutral axis in ultimate state service, which using f_{yb} as a nominal yield characteristic of steel, after being validated in section 8.1 is 8,72mm. Therefore next table contains the distance between each gauge to the neutral axis which is named y:

Gauges	***Distance y (mm)***
1 and 4	33,28
2 and 3	91,28
5	8,72

Table 17 Distance y depending on gauge position.

Next step required to fill the equation 9.1 is knowing the radius of curvature for each d_5 displacement. Figure 49 shows how is developing the midspan flection for curvature as same time as the load cell force is increasing. Using the measurements of each point can be determined the curvature radius with the method explained in section 9.1.1.

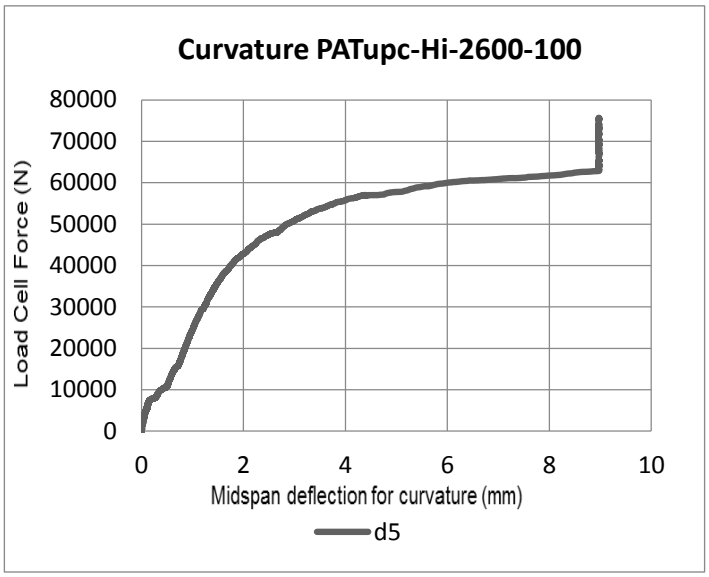

Figure 49 d_5 evolution on new composite slabs

Following table shows the sequence of forces selected to study the strain distribution and the measures of d_5 which permits calculate de radius of curvature. The reason of this selection of forces is the secure range which gauges work.

FORCE(N)	***d5(mm)***	***ρ(mm)***
5000	0,09	1125000
7500	0,16	632812
10000	0,4	253125
15000	0,65	155769
20000	0,85	119118
30000	1,23	82317
40000	1.75	57858

Table 18 Radius of curvature from d_5.

Experimentally, gauges measure deformations associated to strain-force after every period of loading. Next table shows the differences between the theoretical longitudinal normal strain obtained by the formula $\varepsilon_x(y) = \frac{-y}{\rho}$ compared with the commented experimental gauge measurements.

FORCE(N)	***strain***	***g1(με)***	***g2(με)***	***g3(με)***	***g4(με)***	***g5(με)***
5000	$\boldsymbol{\varepsilon_{exp}}$	*5*	*54*	*56*	*4*	*-32*
	$\boldsymbol{\varepsilon_{theoretical}}$	*27*	*81*	*81*	*27*	*-8*
7500	$\boldsymbol{\varepsilon_{exp}}$	*21*	*140*	*134*	*12*	*-44*
	$\boldsymbol{\varepsilon_{theoretical}}$	*52*	*144*	*144*	*52*	*-14*
10000	$\boldsymbol{\varepsilon_{exp}}$	*40*	*380*	*373*	*12*	*-46*
	$\boldsymbol{\varepsilon_{theoretical}}$	*131*	*361*	*361*	*131*	*-35*
15000	$\boldsymbol{\varepsilon_{exp}}$	*59*	*603*	*609*	*27*	*-63*
	$\boldsymbol{\varepsilon_{theoretical}}$	*214*	*586*	*586*	*214*	*-56*
20000	$\boldsymbol{\varepsilon_{exp}}$	*110*	*759*	*774*	*62*	*-97*
	$\boldsymbol{\varepsilon_{theoretical}}$	*279*	*766*	*766*	*279*	*-73*
30000	$\boldsymbol{\varepsilon_{exp}}$	*218*	*1097*	*1154*	*181*	*-148*
	$\boldsymbol{\varepsilon_{theoretical}}$	*404*	*1109*	*1109*	*404*	*-106*
40000	$\boldsymbol{\varepsilon_{exp}}$	*329*	*1577*	*1680*	*309*	*-228*
	$\boldsymbol{\varepsilon_{theoretical}}$	*575*	*1578*	*1578*	*575*	*-151*

Table 19 Differences in different gauges between $\varepsilon_{theoretical}$ and ε_{exp} .

In order to obtain easily the differences between the theoretical strains and the experimental gauges measures, $\varepsilon_{theoretical}$ and ε_{exp} have been illustrate in following figures. The line printed on them would illustrate the perfect correlation between both strains because. The slope of the perfect line is 1.

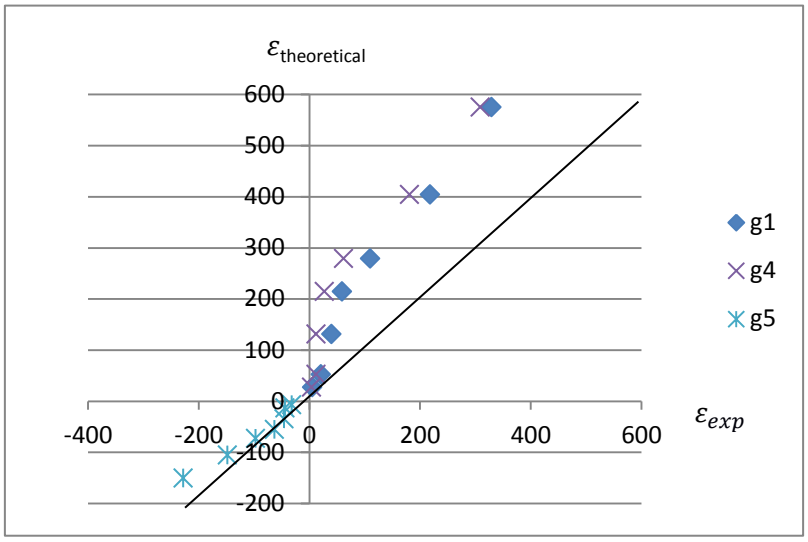

Figure 50 Comparison between $\varepsilon_{theoretical}$ and ε_{exp} in g1, g4 and g5.

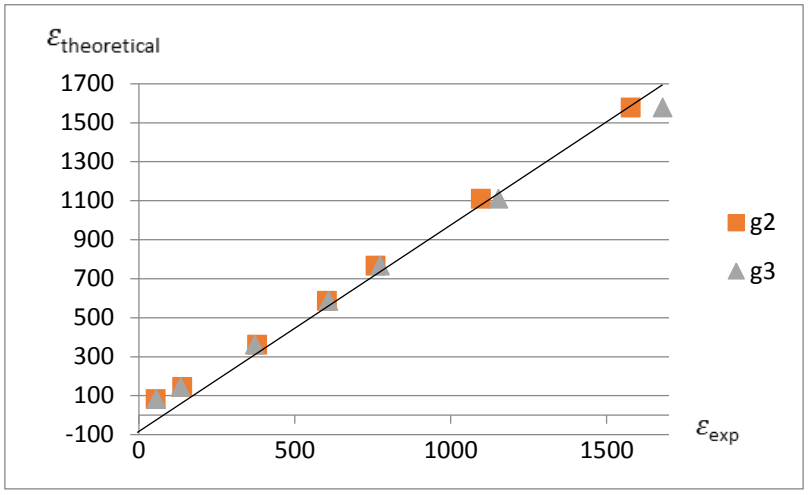

Figure 51 Comparison between $\varepsilon_{theoretical}$ and ε_{exp} in g2 and g3.

As it has been displayed the gauges g2 and g3 have obtained accurated experimental measures if they are compared with the theoretical strain calculated by equation 9.1, and as it is shown in figure 51 how much increase the force, the differences between strains are deeper.

9.1.3. Neutral axis evolution over the slab´s depth

In this section is going to study how evolves the neutral axis experimentally and theoretically around the depth of the slab.

As it has been demonstrated the distance from top to neutral axis x_{pl} should be in the range of 8,72mm to 12,84mm approximately, due to the calculations of ultimate state service.

Following sequence of figures illustrate how evolves the neutral axis over the slab´s depth in full high density punching connection system slabs. On each figure along x-axis is plotted the gauge measurements distributed over the slab´s depth to obtain the experimental elastic calculation and are compared with the theoretical line distribution. And on the ordinate axis is represented the position of each gauge along the slab´s depth.

Some representative load cell forces have been chosen to make the process:

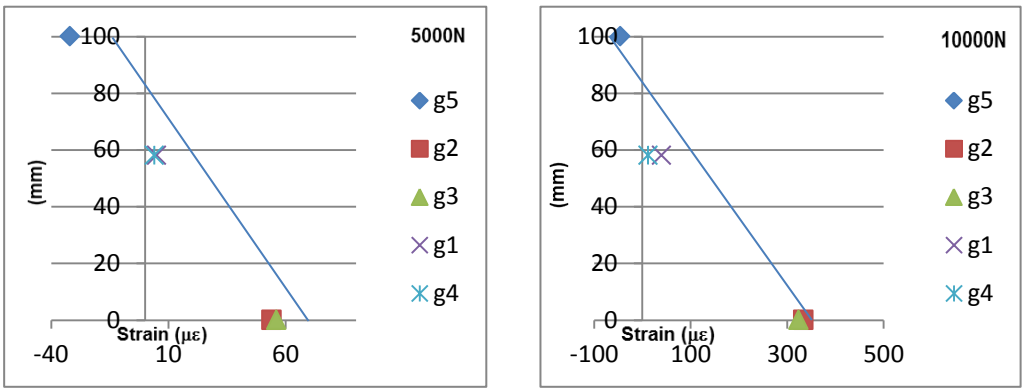

Figure 52 Experimental elastic calculation(F=5000N left, F=10.000 right)

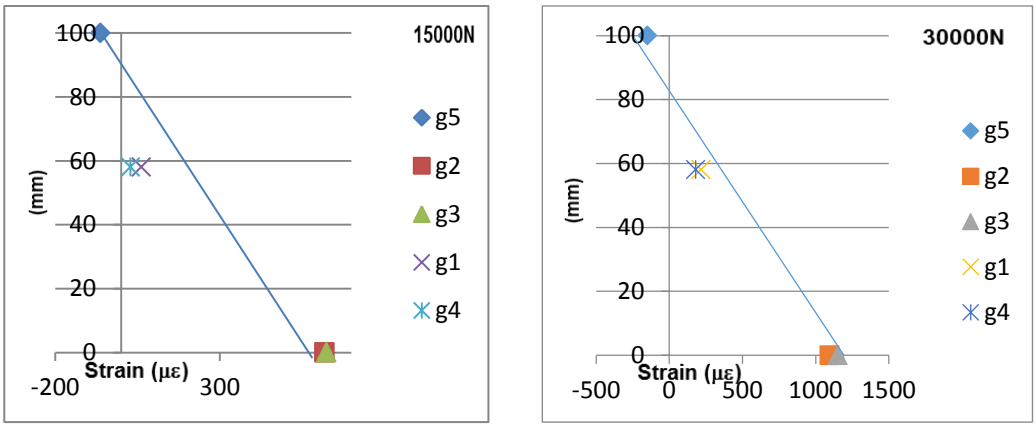

Figure 53 Experimental elastic calculation(F=15.000N left, F=30.000 right)

From these figures is observed how the distance of the experimental elastic calculation of neutral axis remain almost constant during all the process with an approximate values between 12-15mm.

In order to represent the experimental position of neutral axis as much accurate as possible, it has been represented the gauge measurements of the ultimate cell force obtained on testing, which could be assumed as a ultimate state service.

In this case next figure shows how experimental neutral axis is around 12mm from top of the slabs depth, which is in total accordance with the ultimate state x_{pl}=12,84 mm measured by theoretical way in section 8.1.

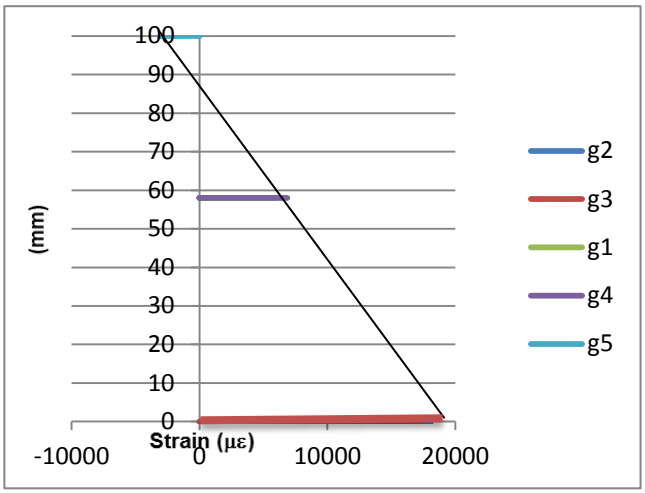

Figure 54 Ultimate strain state

9.2. Deflections

Deflections due to loading applied to the new patent composite slab should be calculated using elastic analysis, neglecting the effects of shrinkage. Additionally, it must be considered that for an internal span of a continuous slab, where the shear connection is achieved, deflection has to be determined using:

- The average value of the cracked and uncracked second moment of area may be taken
- For the concrete, an average value of the modular ratio for long-term and short-term effects may be used

In accordance to BS EN 1994-1-1 calculations of the deflection of the composite slab may be omitted if both the following conditions are satisfied for external or simply supported spans:

- The span/depth ratio of the slab does not exceed certain limits delimited by 20 for a simply-supported span and 26 for an external span of a continuous slab (corresponding to the lightly stressed concrete limits given in EN 1992-1-1.
- The load causing an end slip of 0.5 mm in the (long span) tests on composite slabs exceeds 1.2 times the design service load.

In this section is going to compare the theoretical midspan deflection calculated with following explained method[4][5][6], with the experimental midspan deflection measurements. For this reason is important to know the second moment of area equivalent and Young´s modulus equivalents.

To obtain the second moment firstly is calculated the modular ratio n between steel and concrete taken as the average value of the short and long term modular ratio :

$$n = \frac{E_a}{E'_{cm}} = \frac{E_a}{\frac{1}{2}(E_{cm}+\frac{E_{cm}}{3})} = \frac{E_a}{\frac{2}{3}(E_{cm})} \quad \text{(Eq. 9.3)}$$

with :

E_a : modulus of elasticity of structural steel, in tested value 219000 N/mm^2

E_{cm} : secant modulus of elasticity of concrete, in tested value 29000 N/mm^2

In a cross-section where the concrete in tension is considered as cracked, like the cross-section illustrated in Figure 55 subjected to a sagging moment, the second moment of area I_{cc} can be obtained from:

$$I_{cc} = \frac{b{x_{pl}}^3}{12n} + \frac{b x_{pl}(\frac{x_{pl}}{2})^2}{n} + A_p(d_p - x_{pl})^2 + I_p \quad \text{(Eq. 9.4)}$$

with :

I_p : second moment of area of the profiled sheeting [3]

n : modular ratio

x_{pl} : position of the elastic neutral axis to the upper side of the slab.

For the same section under sagging moment, considering the concrete in tension as not cracked, the second moment of area I_{cu} is given by :

$$I_{cu} = \frac{bh_c{}^3}{12n} + \frac{bh_c(x_u - \frac{h_c}{2})^2}{n} + \frac{b_0 h_p{}^3}{12n} + \frac{b_0 h_p}{n}\left(h_t - x_u - \frac{h_p}{2}\right)^2 + A_p(d_p - x_u)^2 + I_p \quad \text{(Eq. 9.5)}$$

Next figure show all concepts presented in the equation.

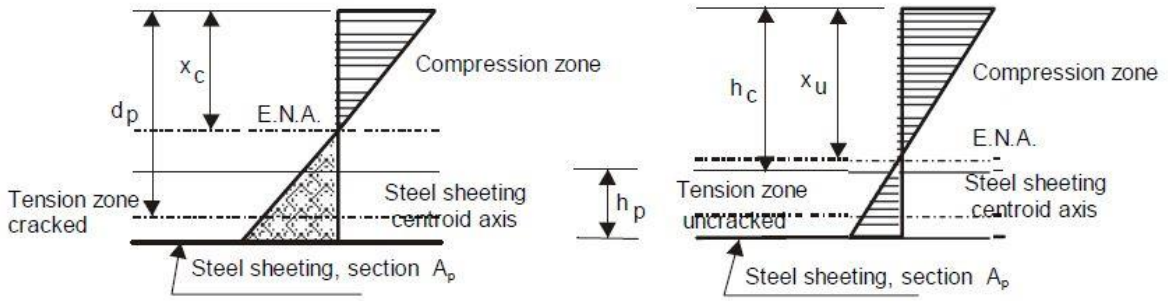

Figure 55 Second moment of area calculation for cracked and uncracked cross-section[17].

In order to simplify the method to calculate the equivalent second moment of area is only considered the most common and real case where the concrete in tension is considered as cracked. The procedure to achieve the theoretical midspan deflection starts calculating the modular ratio n between steel and concrete.

$$n = \frac{E_a}{\frac{2}{3}(E_{cm})} = \frac{219.000}{\frac{2}{3}(29.000)} = 11{,}32$$

In this theoretical case is supposed the constant distance from top to neutral axis of x_{pl}=12,84. Therefore applying all dates already identified on equation 9.2 is obtained next result :

$$I_{cc} = \frac{bx_{pl}{}^3}{12n} + \frac{bx_{pl}(\frac{x_{pl}}{2})^2}{n} + A_p(d_p - x_{pl})^2 + I_p = 3.328.654{,}76 \text{ mm}^4$$

Where I_p is a date from manufacturer of Cofraplus60 I_p=58,79cm^4/m.

Once it is known the second moment of area, to know the equivalent Young´s modulus of the composite slab it has been used the modulus of elasticity of the structural steel due to its higher relevance against the secant modulus of elasticity of concrete working as a composite. From the differential equation of the elastic $\frac{d^2v}{d^2x} = \frac{Mx}{EI}$, supposing the two symmetrical external loads, the theoretical displacement on the midspan is calculated by following formulas:

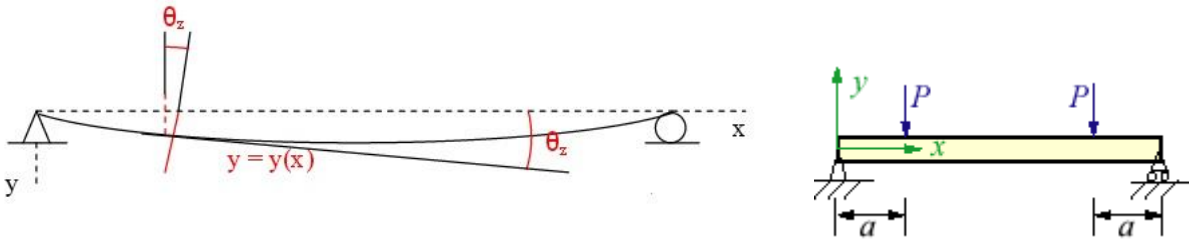

Figure 56 Small deformations diagram[15]

$$\delta = \frac{P \cdot x(3 \cdot a^2 - 3 \cdot L \cdot a + x^2}{6 \cdot E \cdot I} \quad when \quad 0 \leq x \leq a \qquad \text{(Eq. 9.6)}$$

$$\delta = \frac{P \cdot a(a^2 + 3 \cdot x^2 - 3 \cdot L \cdot x}{6 \cdot E \cdot I} \quad when \quad a \leq x \leq L - a \qquad \text{(Eq. 9.7)}$$

$$\delta = \frac{P \cdot (L - x)(3 \cdot a^2 - 3 \cdot L \cdot a + x^2 - 2 \cdot L \cdot x)}{6 \cdot E \cdot I} \quad when \quad L - a \leq x \leq L \qquad \text{(Eq. 9.8)}$$

$$\delta = \frac{P \cdot a(4 \cdot a^2 - 3 \cdot L^2)}{24 \cdot E \cdot I} \quad when \quad x = L/2 \qquad \text{(Eq. 9.9)}$$

$$In\ tested\ case \quad \delta_{midspan} = \frac{(P/2) \cdot (\frac{L}{4})(4 \cdot (L/4)^2 - 3 \cdot L^2)}{24 \cdot E \cdot I} = \frac{M(4 \cdot (L/4)^2 - 3 \cdot L^2)}{24 \cdot E \cdot I} \qquad \text{(Eq. 9.10)}$$

Applying all dates already studied, L=2600mm and EI(stiffness)equivalents, equation 9.10 only depends on the bending moment.

$$\delta_{midspan} = \frac{M(4 \cdot (L/4)^2 - 3 \cdot L^2)}{24 \cdot E \cdot I} = \frac{M \cdot 18.590.000 mm^2}{24 \cdot \frac{219.000N}{mm^2} \cdot 3.328.654 \text{mm}^4}$$

To prove the method is compared the moment resulting from load cell forces of 30.000N, 40.000N and 50.000N.

The corresponding moments of each force are respectively 9,75kNm, 13kNm, 16.25kNm.

$\delta_{midspan\ theoretical}$ (F=30.000N) = 10,37 mm

$\delta_{midspan\ theoretical}$ (F=40.000N) = 14,19 mm

$\delta_{midspan\ theoretical}$ (F=50.000N) = 18,23 mm

Comparing these midspans deflection with the experimental measurements, showed in next figure, it has been proved the effectiveness of the method :

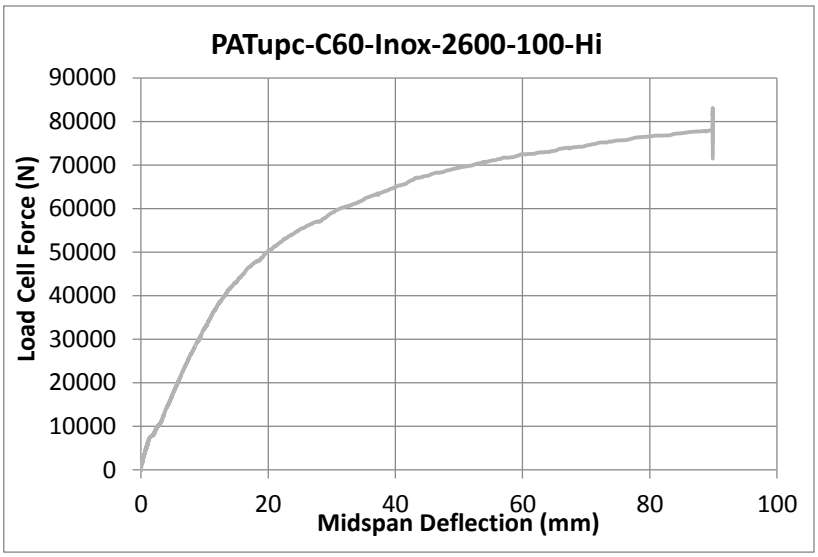

Figure 57 Experimental midspan deflection

9.3. Ultimate force resistance of Cofraplus 60 slabs

In this section is created an ultimate load table, where are included the ultimate resistance forces capable to reach for composite slabs with C60 profile steel sheeting and the new connection system. The table shows the possible different slab measures disposed by Argal ArcelorMittal [16] and it depends on the depth of the slab (h_t) and the distance between supports (L). Following equation is derived from Eq. 5.7 and equalized to bending moment equivalent. Where L(mm) and h_t (mm) are both variables and P(N) is the unknown quantity. The rest of formula´s date are characteristics of the slab.

$$A_p f_{yp}\left(h - 33 - 0.5\left(\frac{A_p f_{yp}}{b f_{cm}}\right)\right) = \frac{PL}{8} \qquad \text{(Eq. 9.11)}$$

To obtain as much real as possible situation, is going to be considered the ultimate tensile strengths instead of medium yield characteristic of steel property in last equation to build the table.

ht/L	2200	2600	3000	3600	4200
180	223291N	188939N	138686N	115571N	99061N
160	191524N	162098N	122864N	102386N	87760N
140	159759N	135179N	107042N	89202N	76458N
120	127989N	108299N	91220N	76017N	65157N
100	102816N	81419N	70563N	58802N	50402N

Table 20 Ultimate load table depending on h_t and L

10. Environmental impact

Construction materials constitute the majority of percentage about humans resources used nowadays. The Worldwatch Institute[12] estimated that world building construction was responsible of 40% of the stone, sand, and gravel, 40% of the energy, and 16% of the water used globally in 1999. Despite the fact that material construction has decreased considerately in last decade, reducing the consumption of construction materials is one of the targets in new buildings designs.

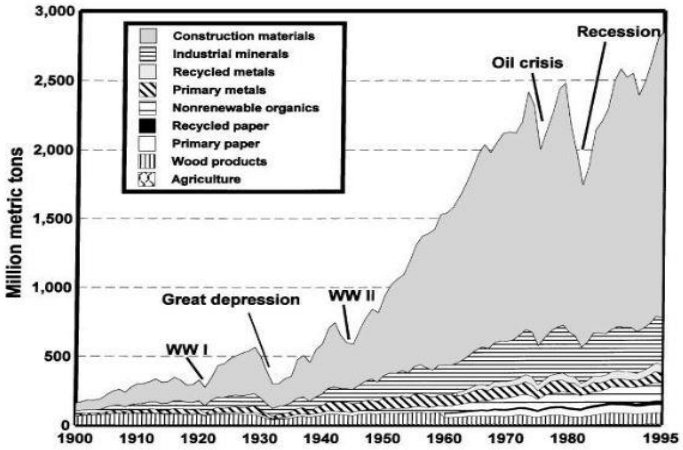

Figure 58 Raw material consumed in USA, until 1995[12]

Concrete and steel are both main row materials in composite slabs. The environmental impact of these materials can be divided in how much energy and CO_2 consumption they have, their resource depletion and waste minimisation.

However, it can also be included human concerning or healthy benefits. For instance the need of incorporate zinc during the galvanization process to achieve galvanized carbon steel in order to assure a minimum fire resistance. The electrolytic production of zinc could produce sulfuric acid and zinc sulfate fogs that are poisonous for humans and could cause diseases as diarrhea, vomit and high fever. A research using stainless steel instead of carbon steel for composite slabs is being carried by the scientific society to avoid these problems.

10.1. Energy consumption and CO_2 emissions

Despite the fact that neither steel or concrete are especially pollutant during its obtaining process, they come with high energy requirements. Buildings consume half of the European Union's the total energy and emit half its annual carbon dioxide production throughout their life cycles.

Amount of researches have studied and compared the energy of production for concrete, steel and other common building materials for raw material extraction, transportation and manufacturing.

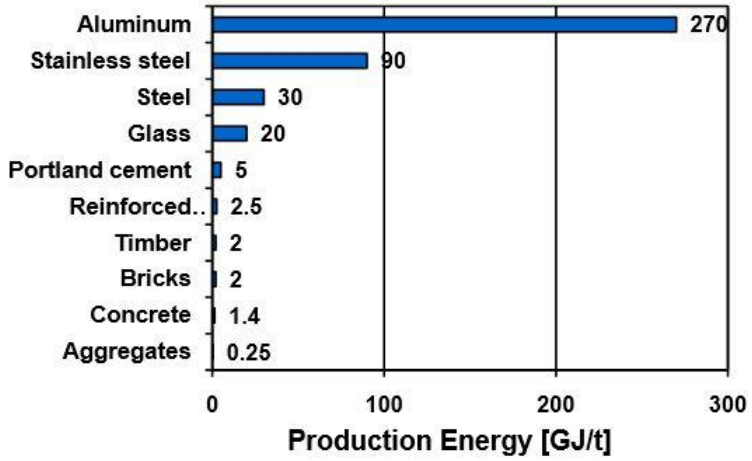

Figure 59 Energy of production for common building materials[13]

The study concludes that the energy required to produce one metric ton of reinforced concrete was 2.5 GJ/t and 30 GJ/t for steel and this puts the steel option at a disadvantage energy-wise.

Despite this difference between these energy consumptions, the amounts of CO_2 embodied in concrete, which are primarily a function of the cement content in the mix designs, are higher than steel because it is estimated that in the worldwide more than 85% of steel is recycled at the end of its life. Such a high figure might seem surprising until one realises that the process is enhanced by steel's natural magnetism, which makes it easy to sort.

Concrete uses about 7% and 15% cement by weight depending on the performance requirements for the concrete. The average quantity of cement is around 250 kg/m^3. One

cubic meter of concrete weighs approximately 2400 kg. As a result, approximately 100 to 300 kg of CO_2 is embodied for every cubic meter of concrete produced or approximately 5% to 13% of the weight of concrete produced, depending on the mix design.

For all these reasons nowadays, there are sustainable initiatives that imply recycled aggregates.

10.2. Waste minimisation

Significant volumes of waste result from activities such as inefficient design, inaccurate materials estimates and orders or design changes are create in traditional concrete slabs. It is notoriously decreased when it is working with composite slabs as structural frames.

Nevertheless the waste created for composite slabs varies depending on the way the composite slab is poured. There are two different pouring ways for composite slabs: pre-casted slabs or in situ pouring. Pre-casted slabs generates less waste than in situ pouring slabs, as it is an industrial process with higher control.
All waste created due to the construction processes needs to be classified in order to facility the recyclability.

Figure 60 Concrete waste

11. Budget

Concept	Unit cost	Amount	Total
Documentation costs	20 €/h	100h	2000 €
Theoretical study	20 €/h	50h	1000 €
Project direction	60 €/h	20h	1200 €
Pc amortization	2 €/h	400h	800 €
Redaction costs	15 €/h	200h	3000 €
Printing and other related costs	70 €/u	1u	70 €

Budget table summarizes all costs found during the development of the project.

The sum of the sub-total is 8070 €

IVA (21%) = 1.681,47 €

The cost total of the project has been = 9751,47 €

Conclusions

The main conclusions of this project are the following:

- The UPC patent new connection system, used on the equivalent Cofraplus60 steel sheeting achieved the total full connection between the steel and the concrete, up to ultimate failure values without slipping at all. Due to this fact the ultimate mean load capable to reach for the new composite slabs using the new UPC system is more than 2 times higher than the mean load capable to reach for same slabs using the conventional embossments system, it means a 100% increase on its behaviour. The force-deflection curve, in addition to the commented fact, it also shows the extremely ductile behaviour of composite slabs with new connection.

- Comparing only the use of ferritic stainless steel and conventional carbon steel as embossed steel sheeting for composite slabs has been shown the similarities in ultimate resistance values. Also it has been proved the reliability of ferritic stainless sheeting when is working on ultimate bending moments, obtaining values very similar to conventional carbon steel. The only noteworthy difference between materials is the resistance force value when first and 0,5 mm slippage occurs, which is lower for traditional carbon steel (ferritic stainless steel approximately ½ of resistance value obtained with carbon steel). The weaker initial adherence would be probably demonstrated because it has an overly smoother surface of stainless steel due to different chemical reaction of the concrete on stainless steel or zinc surfaces.

- Differences on parameters of calculation ultimate limit states services between composite slabs with new connection system and slabs with traditional embossments(ferritic stainless steel and carbon steel), have demonstrated the equations proposed by Eurocode4[4], obtaining total similarities compared with experimental bending results. Regarding to calculation of partial method applied to stainless-steel and conventional steel sheeting, have given similar results of ultimate medium shear stress.

- Strain gauges measurements have corroborated how slabs with the UPC connection system ensure the steel higher yielding and concrete crushes in upper fibres. Moreover they provide the real position of the neutral axis, found it by experimental way. Which is in accordance to the theoretical calculations of ultimate state service on new connection slabs, due to the similar values obtained

- Deflection calculations [4][5][6] have been in accordance to real experimental cases due to vertical detachment or longitudinal did not produce on composite slabs, so the cross-section on tested slabs with new connection has behaved as a theoretical composite section.

.

.

Acknowledgements

I am pleased to recognize Dr. Miquel Ferrer as director of the project, I am really thankful for his help, that I received during all the process and development of the current project. It has been a pleasure to be part of “Departament Resistència de Materials i Estructures a l'Enginyeria. UPC-BarcelonaTech” and have worked with all its database with the aim to study and improve their new Patent in composite slabs.

Bibliography

References

[1] COMITÉ EUROPÉEN DE NORMALISATION. *Eurocode 4: Design of composite steel and concrete structures – Part 1-1 General rules for buildings*. Brusel·les, CEN, 2004

[2] FERRER, M.; MARIMON, F.; GÁMEZ, R. New full connection system for composite slabs: real scale tests. A: European Conference on Steel and Composite Structures. "EUROSTEEL 2014 - 7th European Conference on Steel and Composite Structures". NÀPOLS: 2014, p. 525-526.

[3] FERRER,M; MARIMON,F et alt. Experimental study on longitudinal shear behaviour of composite ferritic stainless steel floor slabs. Univesitat Politècnica de Catalunya. Barcelona, 2014.

[4] EUROCODE 4: Design of composite steel and concrete structures Part1.1 General rules and rules for buildings, EN 1994-1-1:2004

[5] EUROCODE3: Design of steel structures Part 1.3 General rules, Supplementary rules for coldformed members and sheeting, EN 1993-1-3:2004.

[6] EUROCODE 2: Design of concrete structures Part 1.1 General rules and rules for buildings, EN 1992-1-1:2004

[7] JOHNSON, R.P. & ANDERSON, D.: Designers' Guide to EN 1994-1-1: Eurocode 4: Design of Composite Steel and Concrete Structures, Part 1-1: General Rules and Rules for Buildings, Thomas Telford, 2004. .

[8] SERES,N. Numerical modeling of shear connection between concrete slab and sheeting deck. 7th fib international PhD symposium in civil engineering. Stuttgart, 2008.

[9] IL KWANG METAL FORMING Co., Ltd. [http://www.bestmadeinkorea.com/product-34226/Plastic-Processing-Machinery/Roll-Forming-Machine-for-Deck-Plate-Roll-.html, 3 January 1015]

[10] FERRER, MIQUEL. Estudio numérico y experimental de la interacción entre la chapa de acero y el hormigón para la mejora resistente de las losas mixtas frente al deslizamiento longitudinal. Universitat Politècnica de Catalunya. Barcelona, 2006.

[11] UNE EN 12390-3, Ensayos de hormigón endurecido. Parte 3: Determinación de la

resistencia a compresión de probetas.

[12] GRECIA MATOS AND LORIE WAGNER, Consumption of Materials in the United States,1900–1995

[13] NATIONAL READY MIXED CONCRETE ASSOCIATON, *Concrete CO_2 Fact Sheet*, NRMCA Publication Number 2PCO2, February 2012

[14] MONFORT LLEONART J. (2002) *Estructuras mixtas para edificacion segun criterios del Eurocodigo 4*. Valencia.

[15] DOMINGO SANTILLANA, JAIME, *Flexión y deformaciones*, E.P.S.-Zamora – (U.SAL.) - 2008

[16] ARVAL(by ArcerolMittal), *Forjados Cofraplus60, Características geométricas.* [http://ds.arcelormittal.com/repo/lionel%20pezzetti/arval/arval%20template/Downloads%20PDF/Soluciones_Forjados.pdf, 21 November 2014)

[17] EHLERS PETER, Eurocode 4 *Seminar Composite structures Composite Slabs with Profiled Steel Sheeting, University of Aarhus*

[18] MILAN VELJKOVIC, *Behaviour and resistance of composite slabs, Department of civil engineering Lulea University of Tecnology, Sweden 1996*

[19] ES 2344389, EP 2305911, WO 2010037876. "*System for connecting together steel sheet and concrete*".

[20] NAMDEO ADKUJI, LAXMIKANT MADANMAHOCAR GUPTA, *Design of composite slabs with profiled steel decking: a comparison between experimental and analytical studies, International Journal of Advanced Structural Engineering 2012*

Complementary references

FERRER M., MARIMON F., CRISINEL M., 2006. "*Designing cold-formed steel sheets for composite slabs: An experimentally validated FEM approach to slip failure mechanics*". Thin-walled Structures 44 (2006) 1261–1271.

STARK, J.W.B. & BREKELMANS, J.W.P.M.: '*Plastic design of continuous composite slabs', Journal of Constructional Steel Research*, 15, 1990, pp. 23-47.

FERNÀNDEZ, NÚRIA *Estudi teòric i experimental de les lloses mixtes d'hacer inoxidable i formigó* Universitat Politècnica de Catalunya. Barcelona, 2013.

SERES,N., DUNAI,L. *Experimental investigation of an individual embossment for composite floor design.* Concret estructures. 2011.

RITCHIE, J K and CHIEN, E Y L: *Composite floor systems, Constructional Steel Design – An International Guide, Ed. Dowling*, P J et al. Elsevier Applied Science, 1992, pp.471-479

ES 2344389, EP 2305911, WO 2010037876. "*System for connecting together steel sheet and concrete*".

CRISINEL, M. et al. *"Influence of sheet surface conditions and concrete strength on the longitudinal shear resistance of composite slabs*". A Forecast of the Future for Steel and Composite Steel-Concrete Structures – Prof. Jean-Marie Aribert Retirement Symposium, p. 233-244 Rennes, 2006

Structural Applications of Ferritic Stainless Steels (SAFSS). A three year research project funded by the EC's Research Fund for Coal and Steel. 2010-2013.

Porter, M.L.; Ekberg, C.E. "*Coating Effects of Cold-Formed Steel Deck Slabs*". Proceedingd of the 5th International Specialty Conference on Cold-Formed Steel Structures. University of Missouri-Rolda, 1980